ACCOUNTS of chemical research

Article

pubs.acs.org/accounts

Potential of Metal–Organic Frameworks for Separation of Xenon and Krypton

Debasis Banerjee,[†] Amy J. Cairns,[†,∥] Jian Liu,[‡] Radha K. Motkuri,[‡] Satish K. Nune,[‡] Carlos A. Fernandez,[‡] Rajamani Krishna,[§] Denis M. Strachan,[‡] and Praveen K. Thallapally*[,†]

[†]Fundamental & Computational Sciences Directorate, Pacific Northwest National Laboratory, Richland, Washington 99352, United States

[‡]Energy and Environmental Directorate, Pacific Northwest National Laboratory, Richland, Washington 99352, United States

[§]Van't Hoff Institute for Molecular Sciences, University of Amsterdam, Science Park 904, 1098 XH Amsterdam, The Netherlands

Supporting Information

CONSPECTUS: The total world energy demand is predicted to rise significantly over the next few decades, primarily driven by the continuous growth of the developing world. With rapid depletion of nonrenewable traditional fossil fuels, which currently account for almost 86% of the worldwide energy output, the search for viable alternative energy resources is becoming more important from a national security and economic development standpoint. Nuclear energy, an emission-free, high-energy-density source produced by means of controlled nuclear fission, is often considered as a clean, affordable alternative to fossil fuel. However, the successful installation of an efficient and economically viable industrial-scale process to properly sequester and mitigate the nuclear-fission-related, highly radioactive waste (e.g., used nuclear fuel (UNF)) is a prerequisite for any further development of nuclear energy in the near future. Reprocessing of UNF is often considered to be a logical way to minimize the volume of high-level radioactive waste, though the generation of volatile radionuclides during reprocessing raises a significant engineering challenge for its successful implementation. The volatile radionuclides include but are not limited to noble gases (predominately isotopes of Xe and Kr) and must be captured during the process to avoid being released into the environment. Currently, energy-intensive cryogenic distillation is the primary means to capture and separate radioactive noble gas isotopes during UNF reprocessing. A similar cryogenic process is implemented during commercial production of noble gases though removal from air. In light of their high commercial values, particularly in lighting and medical industries, and associated high production costs, alternate approaches for Xe/Kr capture and storage are of contemporary research interest. The proposed pathways for Xe/Kr removal and capture can essentially be divided in two categories: selective absorption by dissolution in solvents and physisorption on porous materials. Physisorption-based separation and adsorption on highly functional porous materials are promising alternatives to the energy-intensive cryogenic distillation process, where the adsorbents are characterized by high surface areas and thus high removal capacities and often can be chemically fine-tuned to enhance the adsorbate–adsorbent interactions for optimum selectivity. Several traditional porous adsorbents such as zeolites and activated carbon have been tested for noble gas capture but have shown low capacity, selectivity, and lack of modularity. Metal–organic frameworks (MOFs) or porous coordination polymers (PCPs) are an emerging class of solid-state adsorbents that can be tailor-made for applications ranging from gas adsorption and separation to catalysis and sensing. Herein we give a concise summary of the background and development of Xe/Kr separation technologies with a focus on UNF reprocessing and the prospects of MOF-based adsorbents for that particular application.

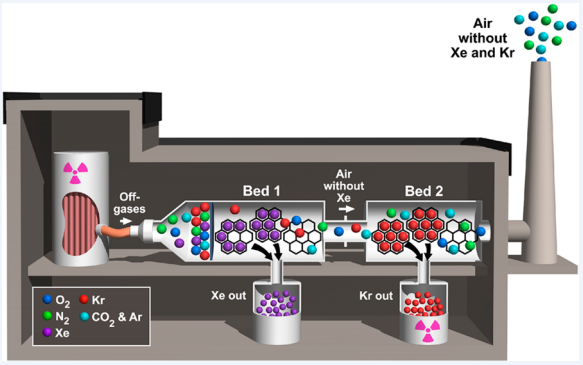

1. INTRODUCTION

The worldwide demand for energy for the transportation and utility sectors continues to be a global interdisciplinary research challenge.[1,2] The need is primarily driven by rapid population and industrial growth, which in turn leads to high energy consumption. Reports from the U.S. Department of Energy (DOE) indicate a ∼28% increase in electrical demand by 2040.[3] It is therefore imperative to devise a highly efficient, safe, and reliable energy solution that can satisfy these increasing demands in a way that does not further harm the land, water, and air.[1,2]

In the United States, electricity is predominately generated from fossil fuels, in addition to nuclear power and renewable energy. Nuclear energy continues to capture attention from both a scientific and political perspective, particularly in light of

Received: August 22, 2014
Published: December 5, 2014

   dx.doi.org/10.1021/ar5003126 | Acc. Chem. Res. 2015, 48, 211–219

the Chernobyl disaster, the Three Mile Island incident, and the more recent 2011 tsunami and subsequent reactor meltdown in Fukushima, Japan.[1] The tsunami impact on the Fukushima nuclear power plant and the surrounding areas prompted officials to revise existing nuclear safety protocols around the world. In spite of these localized incidents, nuclear power remains the leader in emission-free energy production, having an unparalleled energy density compared with other technologies as well as minimal land-use requirements.[1−3] The production of radioactive used nuclear fuel (UNF) during energy generation in a nuclear power plant means that any future success depends on the development of alternative industrial-scale methods to properly sequester and mitigate the UNF. This non-biodegradable waste consists of a mixture of solid high-level waste, liquid low-level waste, and gaseous waste that can take thousands of years to decay, depending on which types of fission and activation products are generated.[4] The majority of UNF is initially stored in deep, water-filled spent-fuel pools with steel-lined concrete walls that are several meters thick. The UNF can be reprocessed after cooling or transferred to leak-tight dry casks for storage until it can be transported to a permanent deep underground geologic repository.[3,4]

In an effort to extend the nuclear fuel supplies, minimize high volumes of radioactive waste, and recover precious isotopes, countries such as France, Japan, and Russia routinely reprocess UNF to recover plutonium and uranium from the irradiated fuel for advanced fuel cycles. However, volatile radionuclides generated during irradiation of the fuel are released into the plant off-gas streams during reprocessing and ultimately into the environment.[4] These radionuclides include but are not limited to noble gases (isotopes of Xe and Kr), ^{3}H, ^{14}C, and ^{129}I. The type of reprocessing method plays a key role in the types of gases that form these radionuclides. For example, in the case of aqueous reprocessing, the off-gas streams contain a mixture of noble gases (predominately ^{85}Kr), tritiated water (^{3}HHO or $^{3}H_2O$), $^{14}CO_2$, and iodine ($H^{129}I$, $^{129}I_2$, and organic iodides).[4] Only ^{3}H and ^{129}I are captured in operating reprocessing facilities, while CO_2 and Kr are released to the environment, resulting in the need to remove radioactive Kr and Xe (if present) when the UNF is reprocessed.

Currently, the United States does not reprocess and recycle UNF because of nuclear proliferation concerns, despite the fact that it has an estimated 70 000 t (and counting) of UNF in storage at nuclear facilities across the country.[4] However, the government does recognize that the current storage technology is not a viable long-term solution, but strict licensing requirements in conjunction with high infrastructure/maintenance costs impede the use of existing reprocessing technologies.

2. XENON AND KRYPTON SEPARATION TECHNOLOGIES: WHERE DO WE STAND?

Nonradioactive xenon-based devices are ubiquitous in our daily lives, ranging from lighting and lasers to medical devices.[5−9] However, while Xe and Kr are volatile noble gases that are available naturally in the atmosphere, they are exceptionally rare compared with other gases, with detectable concentrations of only 0.09 and 1.1 ppm, respectively. Commercially, these gases are removed from air by an energy-intensive cryogenic distillation method. The separation is accomplished on the basis of differences in the boiling point (e.g., −108.12 and −153.22 °C for Xe and Kr, respectively; Figure 1).[10] In light of

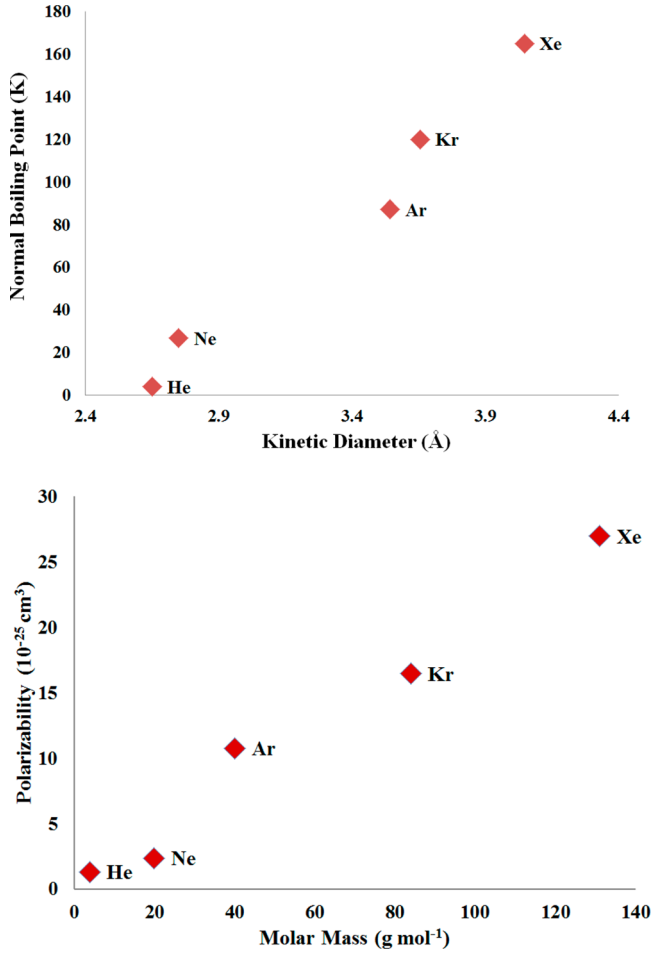

Figure 1. Thermodynamic properties of different noble gases.

the high costs and elevated safety concerns (e.g., possible ozone formation from radiolysis in liquid air), researchers are actively pursuing alternative Xe/Kr capture and storage technologies for off-gas streams.[5−8,11,12] A promising process should be capable of removing Xe and Kr from air and from each other, ideally under ambient temperature and pressure conditions. Typically, UNF would be stored for 5 years or more before being reprocessed. Because of the relatively short half-lives of Xe radionuclides ($t_{1/2}$ = 36.3 days for ^{127}Xe), only nonradioactive Xe would be present when the fuel is reprocessed. However, about 10 mol of Xe is generated during fission for every mole of Kr. Therefore, to minimize the volume of noble gas waste that needs to be stored, Xe should be separated from the Kr and either recovered for sale or released to the environment. Conversely, ^{85}Kr, which has a much longer half-life of 10.8 years, needs to be sequestered and transferred to a storage facility where it would be allowed to decay for a minimum of 110 years before potentially being released into the atmosphere, when the majority of the Kr inventory (about 90%, depending on the age of the fuel) is nonradioactive.

The proposed alternatives for Xe/Kr removal can essentially be divided into two categories: selective absorption by dissolution in a solvent and physical adsorption on porous materials.[5,12,13] In principle, the liquid absorption process would be carried out in a similar manner to cryogenic distillation, but the separation factor is governed by the solubility of the targeted gases in a particular solvent and varies as a function of temperature and pressure. For example, a team

dx.doi.org/10.1021/ar5003126 | Acc. Chem. Res. 2015, 48, 211−219

of researchers achieved ^{85}Kr separation factors of up to 1000 and removal efficiencies of 99.9% by implementing an absorption into dichlorodifluoromethane (refrigerant-12, R-12) as a process solvent.[13,14] This fluorocarbon absorption study was carried out on a pilot scale and offered several advantages, including low solvent and refrigeration costs along with reduced explosion hazards. Nevertheless, in order for this technology to be considered as a viable alternative, the operating pressures would need to be reduced and potential solvent losses from process leakage, volatilization, and radiolysis degradation would need to be addressed. Alternatively, CO_2 was considered as a process solvent and shared many of the advantages offered by fluorocarbon absorption, but this technology is limited to gas streams with elevated CO_2 concentrations.[14]

Separations relying on physisorption onto microporous materials are widely recognized as a promising alternative to absorption-based technologies because the sorbents are characterized by high surface areas that permit enhanced storage capacities and, in some cases, offer the potential to fine-tune the adsorbate−adsorbent interactions in order to optimize the selectivity. Several types of microporous adsorbents have been tested by various research groups for noble gas capture and sequestration. Among these, zeolite molecular sieves are the largest class of commercially available microporous materials, in which corner-sharing tetrahedral TO_4 (T = Al, Si) secondary building units (SBUs) assemble to form extended frameworks with cages, cavities, or channels of suitable size to permit the passage and/or capture of small molecules (<1 nm).[15] Several commercial zeolite molecular sieves have been investigated for noble gas adsorption and separation studies.[12,16] Zeolites such as NaA and NaX have been shown to be selective adsorbents for Xe over Kr (selectivity factors of ∼4−6) but are plagued by low capacities (20−30 wt % at 100 kPa and 25 °C).[16] However, the unique structural characteristics and cost benefits led researchers at Idaho National Laboratory to perform a systematic investigation of Xe/Kr adsorption on mordenite, a synthetic zeolite of general composition $[(Ca,Na_2,K_2)Al_2Si_{10}O_{24}{\cdot}7H_2O]$.[12] Both the protonated (HZ) and silver-exchanged (AgZ) forms bound in a polyacrylonitrile (PAN)-based macroporous polymer (HZ/AgZ-PAN) were evaluated for noble gas adsorption at 191 K and at room temperature. The results indicated that AgZ-PAN exhibits a higher Xe uptake at room temperature compared with HZ-PAN and that the trend reverses at low temperature.[12] Commercially available activated charcoals (or carbons) were also studied by several groups for noble gas adsorption, as they have low cost, high surface area, and high thermal and chemical stability.[17] However, they posed a serious fire-hazard risk due to the presence of NO_x in the off-gas stream. Recently, a solid-state material based on porous organic cages (CC3), whose molecular structure consists of repeating organic building blocks that form three-dimensional cages, has been shown to be an excellent separator of a Xe/Kr mixture from an off-gas stream.[18] Among other solid-state adsorbents, metal−organic frameworks (MOFs), a class of hybrid solid-state crystalline materials with tailor-made architectures, have recently emerged as front-runners for relevant adsorption-related applications.[19−21] The focus of this Account is the recent development and future outlook of MOF-based solid-state microporous adsorbents for adsorption of noble gases (in particular Xe and Kr).

3. METAL−ORGANIC FRAMEWORKS AS SOLID-STATE ADSORBENTS OF NOBLE GASES

MOFs are generally synthesized in situ under mild conditions by directed assembly of prefabricated SBUs in the form of inorganic and organic moieties.[19] Metal ions and/or clusters (i.e., nodes) are bridged together with polyatomic organic linkers (i.e., spacers) to give discrete or extended frameworks. The coordination modes, geometry, directionality, and functionality of the SBUs in conjunction with the synthetic conditions are known factors that govern the underlying topology of the resultant structure.[19] MOFs offer superior advantages over other porous materials (e.g., zeolites, activated carbons, etc.) whereby their hybrid nature and synthetic modularity permit a reticular chemistry approach to target novel materials with diverse chemical compositions, pore sizes, and chemical and thermal stabilities.

Interestingly, the adsorption of noble gases by MOFs remains largely unexplored, with only a handful of experimental and computational proceedings reported in the literature.[5−8,11,22−24] As noted above, the ability to store and separate Xe and Kr by physisorption at ambient pressures and noncryogenic temperatures with zeolites and activated carbons has led to promising results, but they exhibit low uptake capacity. Fine-tuning of the pore properties of these materials for higher capacity is difficult, a shortcoming that the unique attributes of MOFs are well-poised to address! Computational and experimental studies to date have aimed to evaluate the effect of specific structural parameters to enhance noble gas−MOF interactions. To date, several benchmark MOFs have been tested by us and others with encouraging results. Instead of a comprehensive list, brief summaries of representative MOFs and computational studies are discussed below.

3.1. IRMOF-1 (MOF-5)

IRMOF-1 (IRMOF = isoreticular MOF) is a highly porous MOF (surface area = 3100−3800 m^2/g) with tetranuclear $Zn_4O(O_2C)_6$-based SBUs bridged by terephthalate linkers to form a cubic 3-periodic network with squarelike channels with dimensions of ∼1.5 nm.[25] Mueller and co-workers performed the first experimental pressure-swing adsorption (PSA) study to investigate the adsorption performance for storage of Xe and Kr at room temperature.[24] The goal of this study was to prove that a stainless steel container filled with activated MOF-5 contained more moles of rare gases compared with a cylinder without the MOF at the same gas pressure. Their results showed a pronounced difference for gases with higher polarizability, i.e., Xe > Kr > Ar.

3.2. HKUST-1 (Cu-BTC MOF)

HKUST-1 (HKUST = Hong Kong University of Science and Technology) is a 3-periodic Cu-BTC MOF (BTC = benzenetricarboxylate) composed of dimeric Cu(II) paddle-wheel SBUs with two potentially unsaturated metal centers and organic BTC linkers.[26] It is regarded as being an attractive candidate for gas-adsorption applications because of the presence of small and large cavities of internal diameter ∼1.3, 1.1, and 0.5 nm, the accessible open Cu(II) metal sites, and the ease of industrial-scale preparation from inexpensive, commercially available starting materials. Mueller and co-workers performed the first experimental study to investigate the Xe/Kr adsorption selectivity of HKUST-1.[24] In a typical breakthrough experiment, a gas stream containing a mixture of Kr (94%) and Xe (6%) was continuously passed through a reactor

dx.doi.org/10.1021/ar5003126 | Acc. Chem. Res. 2015, 48, 211−219

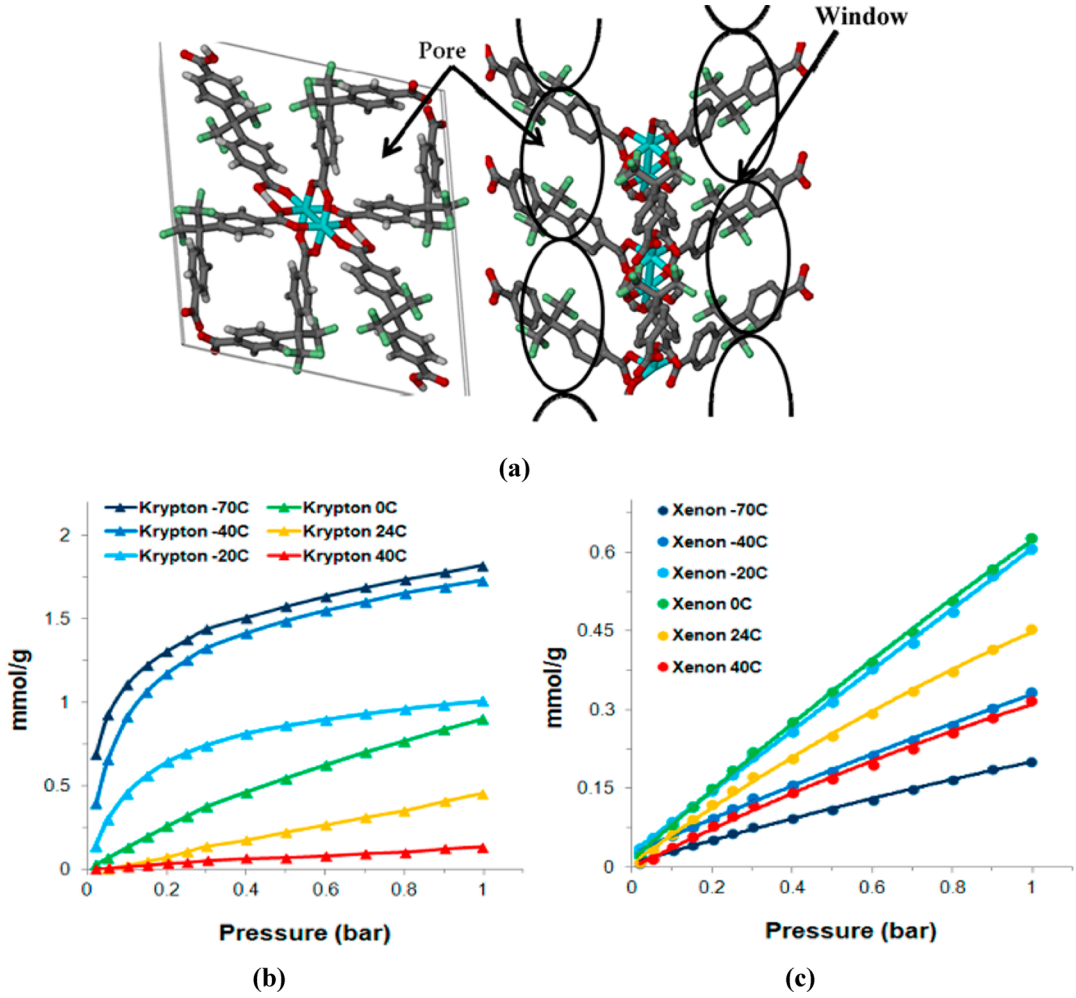

Figure 2. (a) Crystal structure of FMOFCu. The 1D open channels are connected through the bottleneck windows. Color code: Cu, green; C, gray; O, red. All hydrogen atoms and guest molecules have been omitted for clarity. (b, c) Variable-temperature pure-component (b) Kr and (c) Xe adsorption isotherms for FMOFCu collected up to pressures of 1 bar at six temperatures ranging from −70 to 40 °C. Reproduced from ref 22. Copyright 2012 American Chemical Society.

packed with the activated material at 55 °C and 4 MPa. A significant improvement was observed for the Xe/Kr selectivity compared with activated carbons: the Xe concentration measured in the reactor outlet was reduced to 50 ppm because of the preferential adsorption of Xe in the MOF sorbent. We performed a dynamic breakthrough column measurement at 100 kPa and room temperature with pellets of commercially available HKUST-1.[7] The single-component and binary breakthrough curves reveal that this material preferentially adsorbs Xe over Kr. However, the Xe capacity (3.18 mol/kg) was still lower than that of the benchmark activated carbon (3.72 mol/kg). Moreover, the selectivities measured for three gas compositions (i.e., Xe/Kr = 20:80, 50:50, 80:20) were consistently lower than those for activated carbon (e.g., ~2.6 at 100 kPa). Interestingly, in accordance with nuclear fuel reprocessing applications, HKUST-1 was found to selectively adsorb low (ppm) concentrations of Xe and Kr from air (e.g., N_2, 78%; O_2, 21%, Ar, 0.9%; CO_2, 0.03%, etc.) with values comparable to those for activated carbon.[7] To pinpoint the preferred adsorption sites of Xe in HKUST-1 and thereby understand the mechanism of Xe/Kr selectivity, studies were conducted using several analytical techniques including ^{129}Xe NMR spectroscopy, grand-canonical Monte Carlo (GCMC) simulations, and synchrotron neutron and X-ray diffraction.[27,28] These results, most notably those by Hulvey and co-workers, confirmed the location of the favorable Xe adsorption site as being the small pockets and the surrounding windows leading to the cavity. This is in contrast to what was observed for other gases (e.g., H_2, CO_2), where the adsorbate primary interaction site is the accessible unsaturated Cu(II) center.[27]

3.3. FMOFCu

FMOFCu is a twofold-interpenetrated, partially fluorinated Cu-based MOF in which copper paddlewheel SBUs are connected by ditopic V-shaped 4,4′-hexafluoroisopropylidenebis-(benzoate) (hfipbb) linkers to form the overall 3-periodic framework.[22] This particular MOF was specifically selected by us for Xe/Kr adsorption studies because of its potential to exhibit a "molecular sieving" effect. The pore structure contains tubular cavities (ca. 0.51 nm × 0.51 nm) with bottleneck windows having estimated dimensions of 0.35 nm × 0.35 nm. Accordingly, under the appropriate conditions it was possible for Kr to be selectively adsorbed over Xe, as their kinetic diameters are 0.36 and 0.39 nm, respectively. Most porous adsorbents (e.g., zeolites) preferentially adsorb Xe over Kr, a process primarily driven by the higher polarizability of Xe atoms. Indeed, pure-component gas adsorption isotherms confirmed that FMOFCu is selective toward Kr (termed

dx.doi.org/10.1021/ar5003126 | Acc. Chem. Res. 2015, 48, 211−219

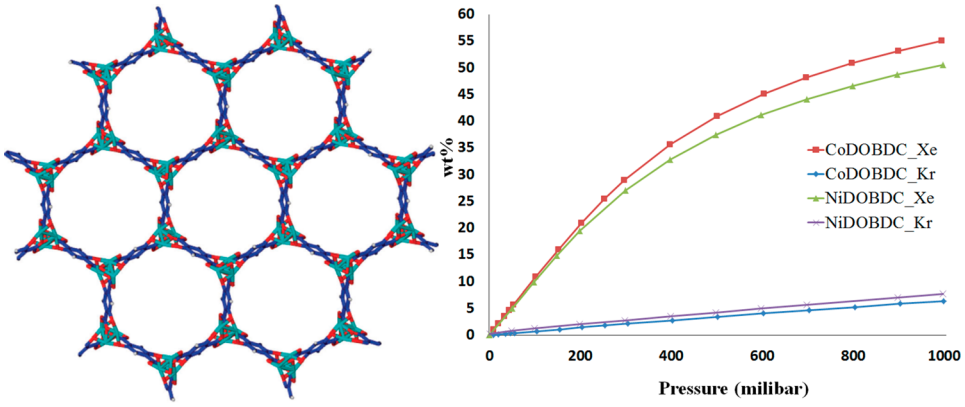

Figure 3. (a) Honeycomb network structure of Ni-DOBDC. (b) Xe and Kr adsorption isotherms at room temperature for M-DOBDC (M = Ni, Co). Reproduced with permission from ref 5. Copyright 2012 Royal Society of Chemistry.

"reverse selectivity"). The behavior was temperature-dependent and observed only below 0 °C (Figure 2).[22] The selectivity was reversed above 0 °C, where the Xe and Kr adsorption capacities were comparable across the entire pressure range. The lowest Xe capacity was observed at −70 °C, probably because of the contraction of the bottleneck windows. The windows appeared to expand and the molecules readily diffused above 0 °C. The "reverse selectivity" behavior was predicted by computational studies, though the example of FMOFCu remains the only experimental report to date.[29,30]

3.4. M-DOBDC (M-MOF-74)

M-DOBDC (M = Mg, Mn, Fe, Co, Ni, Zn; DOBDC = 2,5-dihydroxyterephthalate; MOF-74-M) is a class of isostructural microporous MOFs with regular, hexagonal unidimensional pores decorated with open metal sites at the pore surface.[31] The presence of abundant, accessible open metal sites and the significant porosity (∼1000−1500 m^2/g) leads to excellent adsorption properties for various adsorbates. We carried out adsorption experiments on Ni-DOBDC and found that it has a Xe adsorption capacity of 55 wt % at 100 kPa and 298 K, comparable to that of activated carbon (Figure 3).[5] However, it exhibits a Kr uptake of only 3 wt % under similar experimental conditions. Ni-DOBDC has a high isosteric heat of adsorption (Q_{st}) across a wide range for Xe (22 kJ/mol) and a Xe/Kr selectivity of ∼5−6, twice that of activated carbon. The preferential adsorption of Xe atoms and associated high Q_{st} are believed to be due to the interaction between adsorbed Xe atoms and the accessible open metal sites. The work by Perry and co-workers on the other M-DOBDC (M = Mg, Co, Zn) showed that the adsorption performance and selectivity was largely unaffected by variation of the metal center, as the formal charge and the nature of the interaction remained the same across the series.[9] Eventually, we were able to enhance the uptake capacity and selectivity of Ni-DOBDC with a nanoparticle loading approach.[6] The silver-nanoparticle-loaded Ni-DOBDC (Ag@Ni-DOBDC) had better Xe uptake capacity (70 wt %) and selectivity (Xe/Kr ≈ 7) than the parent framework because of the strong dipole−induced dipole interaction between adsorbed Xe atoms and uniformly dispersed silver clusters within the pores. The high Xe adsorption capacity of Ni-DOBDC and the reverse selectivity of FMOFCu were combined in a two-bed breakthrough measurement in which Xe was removed from the mixture stream first using a Ni-DOBDC bed. The left-over gas stream containing a higher percentage of Kr than the original stream was then flowed over a FMOFCu bed at 233 K to adsorb the Kr. Since most of Xe was captured in the first bed, the competition for the adsorption site in second bed was comparatively low, leading to a higher Kr uptake than usual (Figure 4).[32]

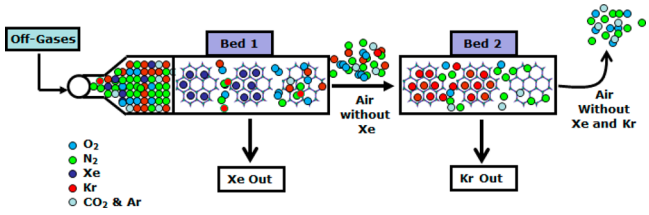

Figure 4. Separation of radioactive Kr from nuclear reprocessing plants using two-column adsorption modules. Reproduced from ref 32. Copyright 2014 American Chemical Society.

3.5. $M_3(HCOO)_6$

Among a diverse range of metal formates, $M_3(HCOO)_6$ (M = Mg, Ni, Co, Zn, Mn) is particularly noteworthy because of its simplistic diamondoid topology and the existence of a zigzag channel with an effective pore size of 0.5 to 0.6 nm.[8,11] The adsorption of Xe in nanoporous $Co_3(HCOO)_6$ shows a type I adsorption isotherm (26 wt % at 25 °C and 100 kPa), while the adsorption isotherm for Kr was found to be linear.[8] As expected from the nature of isotherms, a greater Q_{st} for Xe (29 kJ/mol) than for Kr (22 kJ/mol) was calculated for $Co_3(HCOO)_6$, and similar Q_{st} trends were also observed for the other isostructural metal analogues (Figure 5). The follow-up breakthrough experiments backed up the Xe selectivity (∼6) for the $M_3(HCOO)_6$ series.[8] Simulations showed that each Xe atom optimally fits within a segment (i.e., a zig or a zag) and thus can interact more effectively with the π cloud of the formate groups on the pore surface.[11]

3.6. MOF-505

MOF-505 is a 3-periodic MOF composed of copper paddlewheel SBUs connected by the organic linker biphenyl-3,3′,5,5′-tetracarboxylate (bptc), forming different pore diameters (0.48, 0.71, and 0.95 nm).[23] Bae and co-workers chose MOF-505 on the basis of published simulation studies showing a high Xe/Kr selectivity over the typical operating pressure

dx.doi.org/10.1021/ar5003126 | Acc. Chem. Res. 2015, 48, 211−219

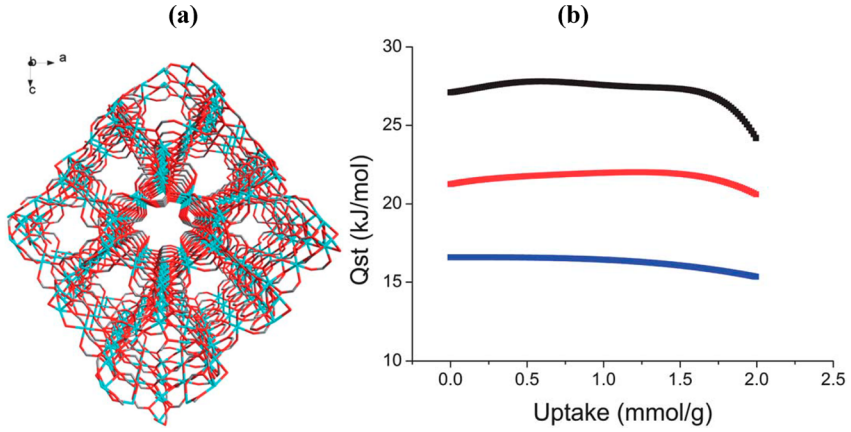

Figure 5. (a) $Co_3(HCOO)_6$ framework along the crystallographic [010] axis. (b) Q_{st} values for xenon (black), krypton (red), and argon (blue) measured at cryogenic temperatures. Reproduced with permission from ref 8. Copyright 2013 Royal Society of Chemistry.

range (0.1 to 1 MPa).[23,29] The breakthrough experiment with a 20:80 mixture of Xe and Kr indicated a much higher retention time for Xe compared with Kr, and the selectivity was calculated to be 9−10, in line with the results of the simulations. The higher Xe selectivity is attributed to the pore confinement effect and the presence of "polarizable" open metal sites of the paddle wheel SBUs at the pore surface.

3.7. Comparison of the Separation Performance of Various MOFs

The separation performance of MOFs in industrial fixed-bed adsorbers is governed by a combination of three factors: (a) adsorption selectivity, (b) uptake capacity, and (c) intracrystalline diffusivities of guest molecules.[33] The selection of MOFs solely on the basis of adsorption selectivity, as is commonly done in published studies, often leads to misleading conclusions.[29] To illustrate this, we consider the separation of 20:80 Xe/Kr mixtures by each of six MOFs: Ni-DOBDC, Ag@Ni-DOBDC, HKUST-1, IRMOF-1, FMOFCu, and $Co_3(HCOO)_6$. The hierarchy of Xe/Kr adsorption selectivities is $Co_3(HCOO)_6$ > Ag@Ni-DOBDC > Ni-DOBDC > HKUST-1 > IRMOF-1 > FMOFCu. The Xe uptake capacities follow a different hierarchy: Ag@Ni-DOBDC > Ni-DOBDC > $Co_3(HCOO)_6$ > HKUST-1 > IRMOF-1 > FMOFCu (Figure 6). Transient breakthrough simulations are potent tools for comparing the separation performance of MOFs because they take proper account of selectivity, uptake capacity, and diffusion limitations. The breakthrough characteristics of 20:80 Xe/Kr mixtures in fixed beds packed with each of the six MOFs are shown in Figure 7 (see the Supporting Information for simulation details). Both IRMOF-1 and FMOFCu are incapable of producing Kr of the desired purity. The longest breakthrough time is obtained with Ag@Ni-DOBDC; consequently, this MOF is the best to produce Kr with the desired purity level (see the Supporting Information for a video animation). The hierarchy of Kr selectivities is Ag@Ni-DOBDC > Ni-DOBDC > $Co_3(HCOO)_6$ > HKUST-1. It should be noted that because of the lower Xe uptake capacity and diffusion limitations, $Co_3(HCOO)_6$, which has the highest Xe/Kr selectivity, performs significantly poorer than Ag@Ni-DOBDC.

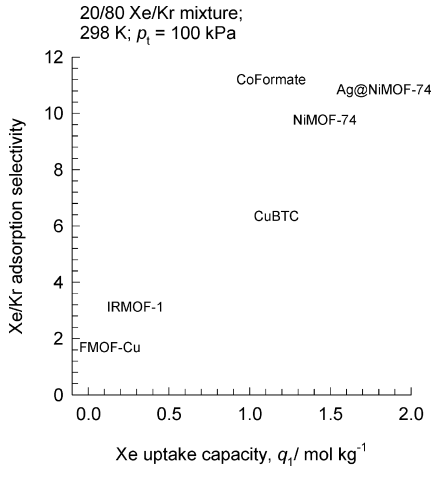

Figure 6. Plot of adsorption selectivity vs uptake Xe capacity.

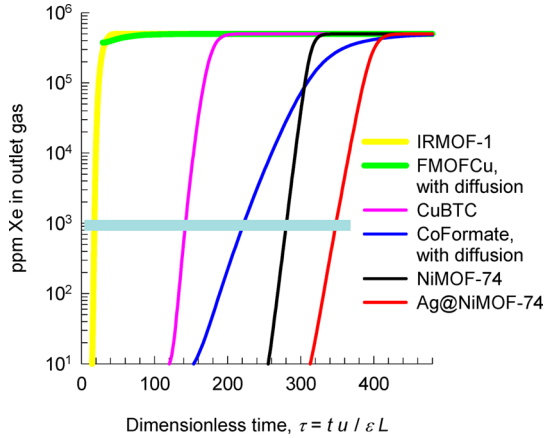

Figure 7. Transient breakthrough simulations showing the concentrations of Xe (in ppm) in the outlet gas mixtures of 20:80 Xe/Kr mixtures exiting fixed-bed absorbers containing various MOFs.

3.8. Computational Studies

The number of potential MOFs for Xe/Kr separation is enormous, with many new novel structures produced weekly. However, because of time constraints and lack of available resources, it is not feasible for experimentalists to systematically screen all MOFs for their gas adsorption behavior. In an effort to alleviate this dilemma, the use of computational methods has gained momentum and provided valuable insight toward the development of structure−property trends that allow the

dx.doi.org/10.1021/ar5003126 | Acc. Chem. Res. 2015, 48, 211−219

adsorption properties for a given material (e.g., capacity, selectivity, diffusion, preferred adsorption sites, etc.) to be simulated for both existing and hypothetical MOFs.[29,30,34] Sikora and co-workers used high-throughput computational methods to generate 137 000 hypothetical MOFs possessing assorted coordination modes, chemical compositions, pore sizes, and morphologies.[30] The Xe/Kr adsorption data generated from GCMC simulations confirmed that the pore size and shape play a fundamental role in governing the adsorbate−MOF interactions. Enhanced selectivity was observed for structures having tubelike uniform pores with diameters large enough to accommodate at most one Xe atom. However, a promising candidate must also exhibit high uptake capacities, and therefore, a fine balance exists between optimal pore size and surface area. This was exemplified by Ryan and co-workers, who performed GCMC simulations on a series of prominent MOFs with diverse chemical and structural characteristics.[29] Not surprisingly, they found that MOFs with higher surface area adsorb larger amounts of Xe and Kr and thus exhibit lower selectivity. Accordingly, among all of the MOFs tested, Pd-MOF is the most selective sorbent for Xe/Kr, but its low adsorption capacity leaves plenty of room for improvement. Given the diverse nature and internal complexity of these materials, employing the computer simulation results is often not straightforward and in many cases involves approximations that have the potential to significantly affect the outcome. In general, reported differences between simulated and experimental results commonly arise from sample preparation and activation procedures and impurities, pore blockage, particle size, and insufficient amount of sample for sorption analysis.[34] From a modeling perspective, differences could be attributed to the applied force field parameters (e.g., rigid vs flexible), taking into account or neglecting polarization, charges, etc. In order to produce high-quality data, it is therefore imperative to perform Brunauer−Emmett−Teller screening measurements to ensure that the appropriate solvent system and activation temperature are employed in order to fully exploit the available porosity of the MOF.

4. FUTURE SCOPE AND OUTLOOK

Porous MOFs are advantageous over other adsorbents because they can be tailored for specific applications. However, as of the date of this article, no large-scale commercial use of MOF-based adsorbents has been reported. Traditionally, MOFs have been envisioned for applications related to carbon capture and sequestration, H_2 storage, and hydrocarbon separation. Since the scale of these applications is enormous, material cost is a major consideration for any practical application. Unlike industrial adsorbents such as zeolites, large-scale production of MOFs is rare. However, with advances in synthetic methodology and appropriate monetary investment in large-scale linker synthesis, MOF prices comparable to those of synthetic zeolites may be possible in the near future. The separation of Xe and Kr during UNF reprocessing is comparatively small-scale, and the cost of the adsorbent material may not have a major impact on the overall cost of a process based on MOFs (though the quality of separation does!). The separation of Xe and Kr in MOF-based solid-state adsorbents occurs as a function of adsorbate size and polarizability. On the basis of our own experimental work on Xe/Kr separation using MOF-based adsorbents, it is clear that an ideal material should have one or more of the following properties: (a) the presence of a high concentration of polar or accessible unsaturated metal centers on the pore surface (e.g., Ni-DOBDC); (b) narrow uniform pores or pockets with diameters that are slightly larger than the kinetic diameter of the adsorbate (e.g., $Co_3(HCOO)_6$, CC3, and FMOFCu); (c) the introduction of polarized nanoparticles within the MOF (e.g., Ag@Ni-DOBDC); (d) temperature-dependent separation of the gas mixture (e.g., FMOFCu). Since it is highly unlikely that one single adsorbent will have all of the desired properties, an optimal MOF-based solid-state adsorbent system for Xe/Kr separation might eventually be obtained by a combination approach in which multiple MOF adsorbents are used to separate and capture Xe and Kr from the flue gas stream. We recently reported such a combination approach where a two-MOF system was used to obtain much higher separation performance. As mentioned previously, MOFs are more selective toward Xe over Kr because of the polarizability difference. However, the presence of excess Xe in the stream means that Xe competes for the same adsorption sites in the MOF as Kr. The use of a material with high Xe adsorption capacity (e.g., Ni-DOBDC) first leads to reduction of the concentration of Xe in the flue gas stream. The gas stream can then be flowed through a second material with high Kr selectivity (e.g., FMOFCu) to capture and sequester Kr from the flue gas. Since Xe is no longer present to compete for sorption sites in the adsorbent in the second material, the capacity and selectivity for Kr increases significantly.[12,32] Apart from the engineering challenges, the use of advanced computer programs to estimate and analyze the selectivities and capacities for MOF adsorbents is a major breakthrough. Computer simulations give direction for experimentalists to narrow their search for potential MOF structures and compositions from the enormous database or to design a new MOF by novel synthetic strategies. The application of computer simulations in predicting tailor-made MOF morphologies is likely to advance in the future with improvements in software and computing power. Finally, the adsorptive separation of Xe and Kr on porous MOFs is a relatively new research area, and relatively few materials have been evaluated to date. The deliberate tuning of the crystal structure and composition using crystal engineering principles, guided by the results of computational studies, to form MOFs that are tailored specifically for the separation of Xe and Kr is likely to yield further fundamental and applied results in the near future.

■ ASSOCIATED CONTENT

Supporting Information

IAST calculations, comparisons of Xe/Kr separations with different MOFs on the basis of breakthrough experiments, transient breakthrough simulations, and a video animation of the transient breakthrough of Xe/Kr with Ag@Ni-DOBDC (AVI). This material is available free of charge via the Internet at http://pubs.acs.org.

■ AUTHOR INFORMATION

Corresponding Author

*E-mail: Praveen.thallapally@pnnl.gov.

Present Address

‖A.J.C.: Aramco Services Company (ASC), Production Technology Team, 16300 Park Row, Houston, Texas 77084, USA.

Author Contributions

The manuscript was written through contributions of all authors. All authors have given approval to the final version of the manuscript.

Notes

The authors declare no competing financial interest.

Biographies

Debasis Banerjee and **Amy J. Cairns** are postdoctoral associates at PNNL working on noble gas separation using porous materials as adsorbents.

Jian Liu, **Radha K. Motkuri**, **Satish K. Nune**, and **Carlos A. Fernandez** are senior scientists at PNNL working on several different research areas involving porous materials.

Rajamani Krishna is a professor at the University of Amsterdam in The Netherlands. He has more than 400 peer-reviewed journal articles on adsorption and diffusion in nanoporous crystalline materials.

Denis M. Strachan is a laboratory fellow at PNNL. His research interests include scientific problems related to nuclear waste management.

Praveen K. Thallapally is a senior scientist at PNNL. His research interests include several aspects of materials chemistry, including adsorptive separation, separation and immobilization of radionuclides (Kr, I_2), and the development of electrooptic-responsive MOFs. He has more than 100 peer reviewed publications in the area of porous materials.

■ ACKNOWLEDGMENTS

We thank the US Department of Energy (DOE), Office of Nuclear Energy, and in particular, J. Bresee, for their support. T. Todd (Idaho National Laboratory) and B. Jubin (Oak Ridge National Laboratory) provided programmatic support and guidance. Pacific Northwest National Laboratory is a multi-program national laboratory operated for the US Department of Energy by Battelle Memorial Institute under Contract DE-AC05-76RL01830.

■ REFERENCES

(1) *International Energy Outlook 2013*; U.S. Energy Information Administration: Washington, DC, 2013.
(2) Hoffert, M. I.; Caldeira, K.; Benford, G.; Criswell, D. R.; Green, C.; Herzog, H.; Jain, A. K.; Kheshgi, H. S.; Lackner, K. S.; Lewis, J. S.; Lightfoot, H. D.; Manheimer, W.; Mankins, J. C.; Mauel, M. E.; Perkins, L. J.; Schlesinger, M. E.; Volk, T.; Wigley, T. M. L. Advanced technology paths to global climate stability: Energy for a greenhouse planet. *Science* **2002**, *298*, 981−987.
(3) *Blue Ribbon Comission on America's Energy Future: Report to the Secretary of Energy*; U.S. Department of Energy: Washington, DC, 2012.
(4) *Strategy for the Management and Disposal of Used Nuclear Fuel and High-Level Radioactive Waste*; U.S. Department of Energy: Washington, DC, 2013.
(5) Thallapally, P. K.; Grate, J. W.; Motkuri, R. K. Facile xenon capture and release at room temperature using a metal−organic framework: A comparison with activated charcoal. *Chem. Commun.* **2012**, *48*, 347−349.
(6) Liu, J.; Strachan, D. M.; Thallapally, P. K. Enhanced noble gas adsorption in Ag@MOF-74Ni. *Chem. Commun.* **2014**, *50*, 466−468.
(7) Liu, J.; Thallapally, P. K.; Strachan, D. Metal−Organic Frameworks for Removal of Xe and Kr from Nuclear Fuel Reprocessing Plants. *Langmuir* **2012**, *28*, 11584−11589.
(8) Wang, H.; Yao, K. X.; Zhang, Z. J.; Jagiello, J.; Gong, Q. H.; Han, Y.; Li, J. The first example of commensurate adsorption of atomic gas in a MOF and effective separation of xenon from other noble gases. *Chem. Sci.* **2014**, *5*, 620−624.
(9) Perry, J. J.; Teich-McGoldrick, S. L.; Meek, S. T.; Greathouse, J. A.; Haranczyk, M.; Allendorf, M. D. Noble Gas Adsorption in Metal−Organic Frameworks Containing Open Metal Sites. *J. Phys. Chem. C* **2014**, *118*, 11685−11698.
(10) Kerry, F. G. *Industrial Gas Handbook: Gas Separation and Purification*; CRC Press: Boca Raton, FL, 2007.
(11) Lawler, K. V.; Hulvey, Z.; Forster, P. M. Nanoporous metal formates for krypton/xenon separation. *Chem. Commun.* **2013**, *49*, 10959−10961.
(12) Soelberg, N. R.; Garn, T. G.; Greenhalgh, M. R.; Law, J. D.; Jubin, R.; Strachan, D. M.; Thallapally, P. K. Radioactive Iodine and Krypton Control for Nuclear Fuel Reprocessing Facilities. *Sci. Technol. Nucl. Install.* **2013**, No. 702496.
(13) Little, D. K.Eby, R. S.Norton, J. L.Patton, J. L.Schultz, R. M.Varagona, J. M. *Noble Gas Removal and Concentration by Combining Fluorocarbon Absorption and Adsorption Techniques*; Oak Ridge Gaseous Diffusion Plant: Oak Ridge, TN, 1982.
(14) *Separation, Storage and Disposal of Krypton-85*; International Atomic Energy Agency: Vienna, 1980.
(15) Breck, D. W. *Zeolite Molecular Sieves: Structure, Chemistry and Use*; John Wiley & Sons: New York, 1974.
(16) Jameson, C. J.; Jameson, A. K.; Lim, H. M. Competitive adsorption of xenon and krypton in zeolite NaA: Xe-129 nuclear magnetic resonance studies and grand canonical Monte Carlo simulations. *J. Chem. Phys.* **1997**, *107*, 4364−4372.
(17) Bazan, R. E.; Bastos-Neto, M.; Moeller, A.; Dreisbach, F.; Staudt, R. Adsorption equilibria of O_2, Ar, Kr and Xe on activated carbon and zeolites: Single component and mixture data. *Adsorption* **2011**, *17*, 371−383.
(18) Chen, L.; Reiss, P. S.; Chong, S. Y.; Holden, D.; Jelfs, K. E.; Hasell, T.; Little, M. A.; Kewley, A.; Briggs, M. E.; Stephenson, A.; Thomas, K. M.; Armstrong, J. A.; Bell, J.; Busto, J.; Noel, R.; Liu, J.; Strachan, D. M.; Thallapally, P. K.; Cooper, A. I. Separation of rare gases and chiral molecules by selective binding in porous organic cages. *Nat. Mater.* **2014**, *13*, 954−960.
(19) Zhou, H. C.; Long, J. R.; Yaghi, O. M. Introduction to Metal−Organic Frameworks. *Chem. Rev.* **2012**, *112*, 673−674 and references therein.
(20) Kitagawa, S.; Kitaura, R.; Noro, S. Functional porous coordination polymers. *Angew. Chem., Int. Ed.* **2004**, *43*, 2334−2375.
(21) Férey, G. Hybrid porous solids: Past, present, future. *Chem. Soc. Rev.* **2008**, *37*, 191−214.
(22) Fernandez, C. A.; Liu, J.; Thallapally, P. K.; Strachan, D. M. Switching Kr/Xe Selectivity with Temperature in a Metal−Organic Framework. *J. Am. Chem. Soc.* **2012**, *134*, 9046−9049.
(23) Bae, Y. S.; Hauser, B. G.; Colon, Y. J.; Hupp, J. T.; Farha, O. K.; Snurr, R. Q. High xenon/krypton selectivity in a metal−organic framework with small pores and strong adsorption sites. *Microporous Mesoporous Mater.* **2013**, *169*, 176−179.
(24) Mueller, U.; Schubert, M.; Teich, F.; Puetter, H.; Schierle-Arndt, K.; Pastre, J. Metal−organic frameworks—Prospective industrial applications. *J. Mater. Chem.* **2006**, *16*, 626−636.
(25) Li, H.; Eddaoudi, M.; O'Keeffe, M.; Yaghi, O. M. Design and synthesis of an exceptionally stable and highly porous metal−organic framework. *Nature* **1999**, *402*, 276−279.
(26) Chui, S. S. Y.; Lo, S. M. F.; Charmant, J. P. H.; Orpen, A. G.; Williams, I. D. A chemically functionalizable nanoporous material $[Cu_3(TMA)_2(H_2O)_3]_n$. *Science* **1999**, *283*, 1148−1150.
(27) Hulvey, Z.; Lawler, K. V.; Qao, Z. W.; Zhou, J.; Fairen-Jimenez, D.; Snurr, R. Q.; Ushakov, S. V.; Navrotsky, A.; Brown, C. M.; Forster, P. M. Noble Gas Adsorption in Copper Trimesate, HKUST-1: An Experimental and Computational Study. *J. Phys. Chem. C* **2013**, *117*, 20116−20126.
(28) Bohlmann, W.; Poppl, A.; Sabo, M.; Kaskel, S. Characterization of the metal−organic framework compound Cu_3(benzene-1,3,5-

tricarboxylate)$_2$ by means of ^{129}Xe nuclear magnetic and electron paramagnetic resonance spectroscopy. *J. Phys. Chem. B* **2006**, *110*, 20177−20181.
(29) Ryan, P.; Farha, O. K.; Broadbelt, L. J.; Snurr, R. Q. Computational Screening of Metal−Organic Frameworks for Xenon/Krypton Separation. *AIChE J.* **2011**, *57*, 1759−1766.
(30) Sikora, B. J.; Wilmer, C. E.; Greenfield, M. L.; Snurr, R. Q. Thermodynamic analysis of Xe/Kr selectivity in over 137 000 hypothetical metal−organic frameworks. *Chem. Sci.* **2012**, *3*, 2217−2223.
(31) Caskey, S. R.; Wong-Foy, A. G.; Matzger, A. J. Dramatic Tuning of Carbon Dioxide Uptake via Metal Substitution in a Coordination Polymer with Cylindrical Pores. *J. Am. Chem. Soc.* **2008**, *130*, 10870−10871.
(32) Liu, J.; Fernandez, C. A.; Martin, P. F.; Thallapally, P. K.; Strachan, D. M. A Two-Column Method for the Separation of Kr and Xe from Process Off-Gases. *Ind. Eng. Chem. Res.* **2014**, *53*, 12893−12899.
(33) Krishna, R. The Maxwell−Stefan description of mixture diffusion in nanoporous crystalline materials. *Microporous Mesoporous Mater.* **2014**, *185*, 30−50.
(34) Van Heest, T.; Teich-McGoldrick, S. L.; Greathouse, J. A.; Allendorf, M. D.; Sholl, D. S. Identification of Metal−Organic Framework Materials for Adsorption Separation of Rare Gases: Applicability of Ideal Adsorbed Solution Theory (IAST) and Effects of Inaccessible Framework Regions. *J. Phys. Chem. C* **2012**, *116*, 13183−13195.

Supporting Information to accompany

Potential of Metal–Organic Frameworks for Separation of Xenon and Krypton

Debasis Banerjee, [a] Amy J. Cairns, [a,#] Jian Liu, [b] Radha K. Motkuri, [b] Satish K. Nune, [b] Carlos A. Fernandez, [b] Rajamani Krishna, [c] Denis M. Strachan [b] Praveen K. Thallapally [a,*]

(a) Fundamental & Computational Sciences Directorate, Pacific Northwest National Laboratory, Richland, WA 99352, USA.

(b) Energy and Environmental Directorate, Pacific Northwest National Laboratory, Richland, WA 99352, USA.

(c) Van't Hoff Institute for Molecular Sciences, University of Amsterdam, Science Park 904, 1098 XH Amsterdam, Netherlands.

[#]Current Address: Aramco Services Company (ASC), Production Technology Team, 16300 Park Row, Houston, Texas USA 77084

ABSTRACT

For any chosen MOF, the Xe/Kr separation characteristics depends on a combination of three separate factors: (a) adsorption selectivity, (b) uptake capacity, and (c) intra-crystalline diffusivities of guest molecules. We compare the performance of some selected MOFs [Ni-DOBDC, Ag@Ni-DOBDC, HKUST-1, IRMOF-1, FMOFCu and $Co_3(HCOO)_6$] in fixed bed operations in order to demonstrate the influence of each of the three separate factors.

For MOFs such as $Co_3(HCOO)_6$ and FMOFCu, in which the guest molecules are strongly confined, intra-crystalline diffusion effects are significant. Such diffusional effects result in distended breakthrough characteristics that have been observed in breakthrough experiments; distended breakthroughs result in lower productivities. Ni-DOBDC, Ag@Ni-DOBDC, HKUST-1 and IRMOF-1 have significantly larger characteristic pore dimensions and diffusional effects are of minor importance for these MOFs. Each of the guest molecules displays sharp breakthrough characteristics for Ni-DOBDC, Ag@Ni-DOBDC, HKUST-1, and IRMOF-1 and intra-crystalline diffusion does not significantly reduce the productivities of desired pure products. On the basis of our analysis, we conclude that Ag@Ni-DOBDC is the best MOF for Xe/Kr separations. $Co_3(HCOO)_6$, that has the highest Xe/Kr selectivity, has a significantly lower productivity than Ag@Ni-DOBDC because of strong diffusional influences.

Table of Contents

Preamble

In this Supporting Information accompanying the manuscript *Potential of Metal-Organic Frameworks for Separation of Xenon and Krypton*, we provide background information on breakthrough simulations. Breakthrough simulations are used to demonstrate that the separation of noble gas mixtures is influenced by three different factors: (a) adsorption selectivity, (b) uptake capacity, and (c) intra-crystalline diffusivities of guest molecules. For illustration purposes five different MOFs are evaluated in detail for the specific task of separating Xe/Kr mixtures: Ni-DOBDC (also known as Ni-MOF-74, CPO-27-Ni; dobdc = 2,5-dioxido-1,4-benzenedicarboxylate),[1, 2] Ag@Ni-DOBDC,[2] HKUST-1,[1, 3] IRMOF-1,[3] FMOFCu,[4] and $Co_3(HCOO)_6$.[5]

Introduction

The noble gases Helium (He), Neon (Ne), Argon (Ar), Krypton (Kr), and Xenon (Xe) have a wide range of practical applications. The main objective of this accounts article is to discuss improved processes for recovery of each of these gases in nearly pure form. Fig. S1 presents data on the molar masses, kinetic diameters, boiling points and polarizabilities, α, of noble gases (He, Ne, Ar, Kr, Xe). We note that the boiling points are He: 4 K, Ne: 27 K, Ar: 87 K, Kr: 119 K, Xe: 165 K. While the differences in boiling points allow us to recover noble gases by fractional distillation, these processes need to operate under cryogenic conditions. The energy demands of cryogenic distillation are particularly severe because of the need to vaporize and condense mixtures at sub-ambient temperatures in reboilers and condensers. Separation of noble gases can also be effected by exploiting the differences in the diameters of atoms. Diffusivities of the noble gases in cage-type zeolites such as DDR, and CHA that have narrow windows in the 3.4 Å – 4 Å range are strongly influenced by the molecular sizes.[6] Differences in the inter-cage hopping rates lead to significant differences in permeation fluxes across microporous membranes.[7] However, an important disadvantage of membrane separations is that high product purities are difficult to achieve; such purities are possible with cryogenic distillation. Selective adsorption within microporous crystalline materials such as metal-organic frameworks (MOFs) offers energy-efficient alternatives to distillation. Adsorptive separations of mixtures of noble gases rely essentially on differences in the polarizabilities of molecules. The value of α generally increases with the molar mass because more electrons are available for polarization (see Fig. S1).

As illustration of the efficacy of MOFs for separation of noble gases, Fig. S2(a) presents pulse chromatographic simulations for separation of a 5-component mixture of noble gases He/Ne/Ar/Kr/Xe in a fixed bed of HKUST-1 operating at 298 K and a total pressure of 100 kPa; the simulation methodology is discussed in a following section. The times at which each of the pulses peak correlates with the corresponding polarizability of the noble gas [see Fig. S2(b)]. In this review, we focus on Xe/Kr mixture separations.

IAST Calculation of Adsorption Selectivities and Xe Uptake Capacities for Binary Xe/Kr Mixtures

Let us examine Xe(1)/Kr(2) separations and compare the performances of Ni-DOBDC, Ag@Ni-DOBDC, HKUST-1, IRMOF-1, FMOFCu, and $Co_3(HCOO)_6$. The adsorption selectivities defined by

$$S_{ads} = \frac{q_1/q_2}{p_1/p_2} \qquad (1)$$

were determined using the pure component isotherm fits along with the Ideal Adsorbed Solution Theory (IAST) of Myers and Prausnitz.[8] Fig. S3(a) presents a comparison the adsorption selectivities for 20/80 Xe(1)/Kr(2) mixtures as a function of the total gas pressure $p_t = p_1 + p_2$. We note that the hierarchy of adsorption selectivities, S_{ads}, is $Co_3(HCOO)_6$ > Ag@Ni-DOBDC > Ni-DOBDC> HKUST-1 > IRMOF-1 > FMOFCu. The Xe uptake capacities, q_1, in the mixtures follow a different hierarchy: Ag@Ni-DOBDC > Ni-DOBDC > $Co_3(HCOO)_6$ > HKUST-1 > IRMOF-1 > FMOFCu [see Fig. S3(b)]. At a total gas pressure pt = 100 kPa, Fig. S3(c) compares S_{ads} and q_1. We note that both IRMOF-1 and FMOFCu suffer from low selectivities and low uptake capacities.

Simulation Methodology for Transient Breakthrough in Fixed-Bed Adsorbers

The separation of Xe/Kr mixtures is commonly carried out in fixed bed adsorbers in which the separation performance is dictated by a combination of three separate factors: (a) adsorption selectivity, (b) uptake capacity, and (c) intra-crystalline diffusivities of guest molecules within the pores. Transient breakthrough simulations are required for a proper evaluation of MOFs; the simulation methodology used in our work is described in earlier publications.[9, 10] A brief summary of the simulation methodology is presented below.

Assuming plug flow of an *n*-component gas mixture through a fixed bed maintained under isothermal conditions (see schematic in Fig. S**4**), the partial pressures in the gas phase at any position and instant of time are obtained by solving the following set of partial differential equations for each of the species *i* in the gas mixture.[11]

$$\frac{1}{RT}\frac{\partial p_i(t,z)}{\partial t} = -\frac{1}{RT}\frac{\partial\left(v(t,z)\,p_i(t,z)\right)}{\partial z} - \frac{(1-\varepsilon)}{\varepsilon}\rho\frac{\partial \bar{q}_i(t,z)}{\partial t}; \quad i = 1,2,...n \qquad (2)$$

In equation (2), t is the time, z is the distance along the adsorbers, ρ is the framework density, ε is the bed voidage, v is the interstitial gas velocity, and $\bar{q}_i(t,z)$ is the *spatially averaged* molar loading within the crystallites of radius r_c, monitored at position z, and at time t.

At any time t, during the transient approach to thermodynamic equilibrium, the spatially averaged molar loading within the crystallite r_c is obtained by integration of the radial loading profile

$$\bar{q}_i(t) = \frac{3}{r_c^3}\int_0^{r_c} q_i(r,t) r^2 dr \tag{3}$$

For transient binary uptake within a crystal at any position and time with the fixed bed, the radial distribution of molar loadings, q_i, within a spherical crystallite, of radius r_c, is obtained from a solution of a set of differential equations describing the uptake

$$\frac{\partial q_i(r,t)}{\partial t} = -\frac{1}{\rho}\frac{1}{r^2}\frac{\partial}{\partial r}\left(r^2 N_i\right) \tag{4}$$

The molar flux N_i of component i is described by the simplified version of the Maxwell-Stefan equations in which both correlation effects and thermodynamic coupling effects are considered to be of negligible importance[10]

$$N_i = -\rho Đ_i \frac{\partial q_i}{\partial r} \tag{5}$$

Summing equation (**3**) over all n species in the mixture allows calculation of the *total average* molar loading of the mixture within the crystallite

$$\bar{q}_t(t,z) = \sum_{i=1}^{n} \bar{q}_i(t,z) \tag{6}$$

The *interstitial* gas velocity is related to the *superficial* gas velocity by

$$v = \frac{u}{\varepsilon} \tag{7}$$

For convenience, the set of equations describing the fixed bed absorber are summarized in Fig. S5. Further details of the numerical procedures used in this work, are provided by Krishna and co-workers.[11-13]

In industrial practice, the most common operation uses a step-wise input of mixtures to be separated into an absorber bed that is initially free of adsorbates, i.e. we have the initial condition

$$t = 0; \quad q_i(0,z) = 0 \tag{8}$$

At time, $t = 0$, the inlet to the absorber, $z = 0$, is subjected to a step input of the n-component gas mixture and this step input is maintained till the end of the adsorption cycle when steady-state conditions are reached.

$$t \geq 0; \quad p_i(0,t) = p_{i0}; \quad u(0,t) = u_0 \tag{9}$$

where u_0 is the superficial gas velocity at the inlet to the absorber.

For simulation of pulse chromatographic separations, such as that presented in Fig. S2(a), we use the corresponding set of inlet conditions

$$0 \leq t \leq t_0; \quad p_i(0,t) = p_{i0}; \quad u(0,t) = u_0 \tag{10}$$

where the time for duration of the pulse is t_0. This type of simulation is particularly useful to demonstrate the fractionating capability of adsorbents.

The breakthrough characteristics for any component are essentially dictated by two sets of parameters:

(a) The characteristic contact time $\frac{L}{v} = \frac{L\varepsilon}{u}$ between the crystallites and the surrounding fluid phase, and

(b) $\frac{Đ_i}{r_c^2}$, that reflect the importance of intra-crystalline diffusion limitations. It is common to use the dimensionless time, $\tau = \frac{tu}{L\varepsilon}$, obtained by dividing the actual time, t, by the characteristic time, $\frac{L\varepsilon}{u}$ when plotting simulated breakthrough curves.[9]

If the value of $\frac{Đ_i}{r_c^2}$ is large enough to ensure that intra-crystalline gradients are absent and the entire crystallite particle can be considered to be in thermodynamic equilibrium with the surrounding bulk gas phase at that time t, and position z of the absorber

$$\bar{q}_i(t,z) = q_i(t,z) \tag{11}$$

The molar loadings at the *outer surface* of the crystallites, i.e. at $r = r_c$, are calculated on the basis of adsorption equilibrium with the bulk gas phase partial pressures p_i at that position z and time t. The adsorption equilibrium can be calculated on the basis of the IAST. The assumption of thermodynamic equilibrium at every position z, and any time t, i.e. invoking Equation (11), generally results in sharp breakthroughs for each component. Sharp breakthroughs are desirable in practice because this would result in high productivity of pure products. Essentially, the influence of intra-crystalline diffusion is to reduce the productivity of pure gases.

Investigating the Influence of Intracrystalline Diffusion

Wang et al.[5] have demonstrated the efficacy of $Co_3(HCOO)_6$ for Xe/Kr separations. Wang et al.[5] postulate that the selective adsorption of Xe is attributable to its commensurate positioning within the cages of $Co_3(HCOO)_6$. This commensurate positioning also necessarily implies that the intra-crystalline diffusivity of Xe will be significantly lower than that of Kr. The experimental breakthrough reported by Wang et al.[5] for 10/90 Xe/Kr mixtures at 298 K and 100 kPa in a bed packed with $Co_3(HCOO)_6$ indicates quite clearly that the breakthrough characteristics of Xe and Kr are significantly different. Kr displays a sharp breakthrough that is typical for species that do not suffer intra-crystalline diffusion limitations. The experimental breakthrough characteristics of Xe, on the other hand has a distended character [see Fig. S6(a)].

Fig. S6(b) presents the transient breakthrough simulations using the data inputs corresponding to the experiments of Wang et al.[5]. The experimental breakthroughs are reproduced, nearly quantitatively, by transient breakthrough simulations that include the influence of intra-crystalline effects with the chosen values $Đ_{Xe}/r_c^2 = 2\times10^{-3}$ s^{-1}; $Đ_{Kr}/r_c^2 = 1\times10^{-2}$ s^{-1}. We note that the diffusivity of Xe within the pores is a factor five lowers than that of Kr because of the much more strongly confined Xe that adsorbs commensurately within the cages of $Co_3(HCOO)_6$. If intra-crystalline diffusional influences are ignored and adsorption equilibrium is assumed to prevail at every position z, and any time t, i.e. invoking Equation (11), we obtain the sharp breakthroughs represented by the dashed lines in Fig. S6(b).

The experimental breakthroughs for 50/50 Xe/Kr mixtures at 298 K and 100 kPa in a bed packed with FMOFCu are reported by Fernandez et al;[4] (see Fig. S9 in the supporting information of ref. 4). We note that the experimental breakthroughs of either component, Xe and Kr, have distended characteristics. The essential characteristics of the breakthroughs are captured by inclusion of intra-crystalline diffusion limitations using the diffusivity values of $Đ_{Xe}/r_c^2 = 2\times10^{-3}$ s^{-1}; $Đ_{Kr}/r_c^2 = 1\times10^{-2}$ s^{-1}, identical to that used for $Co_3(HCOO)_6$ (see Fig. S7). For comparisons, the dashed lines in Fig. S7 indicated simulations without intra-crystalline diffusion limitations. In this case we note the sharp, near-vertical, breakthroughs.

The major conclusions that we draw from the analysis presented in Figs. S6 and S7 is that for MOFs that have relatively small pore sizes, intra-crystalline diffusion are of significant importance. Furthermore, Xe that has the larger size is more strongly constrained and has a lower diffusivity. This results in strongly distended breakthrough characteristics for Xe.

MOFs such as Ni-DOBDC, IRMOF-1 and HKUST-1 have large characteristics pore dimensions and the guest molecules are not strongly constrained. The intra-crystalline diffusivities are expected to be about 10 – 100 times larger than in MOFs such as $Co_3(HCOO)_6$ and FMOFCu. To seek experimental verification of this conclusion let us consider the experimental data of Liu et al.[1] For breakthroughs of

pure Xe and pure Kr in fixed bed packed with Ni-DOBDC operating at 100 kPa and 298 K, the experimental breakthroughs of both Xe and Kr are fairly sharp. Figs. S8(a) and S8(b) present comparisons of the experimental data on pure component breakthroughs with simulations including intra-crystalline diffusion effects (continuous solid lines) with chosen diffusivity values are $Đ_{Xe}/r_c^2 = 2\times10^{-2}$ s^{-1}; $Đ_{Kr}/r_c^2 = 5\times10^{-2}$ s^{-1}. These diffusivity values are about an order of magnitude larger than those chosen for Co Formate and FMOFCu in the foregoing simulations. The dashed lines in Figs S8(a) and S8(b) are simulations in which intra-crystalline diffusional effects are ignored; such equilibrium simulations are slightly sharper than those obtained from simulations that include diffusional effects. The conclusion we draw from Figs. S8(b) and S8(c) is that neglecting intra-crystalline diffusion provides an adequate description of the breakthrough characteristics of Xe and Kr in Ni-DOBDC. Ni-DOBDC has 1D hexagonal-shaped channels of 11 Å size, and a detailed analysis by Krishna[10] has confirmed that diffusional effects can be ignored for the analysis of the breakthrough experiments of Liu et al.[14] for CO_2/N_2 mixtures in Ni-DOBDC.

Liu et al.[1] reported experimental breakthrough data for 20/80 Xe/Kr mixtures at 298 K and 100 kPa in a bed packed with HKUST-1 (see Fig. S8 of the Supporting Information of ref. 1). The experimental breakthroughs are sharp and indicative of negligible intra-crystalline diffusion limitations. We shall verify this conclusion regarding diffusional effects in HKUST-1. Fig. S9 compares the breakthrough characteristics without intra-crystalline diffusion limitations (dashed lines) with breakthrough simulations that include intra-crystalline diffusion effects (continuous solid lines), using the same diffusivity values as for Ni-DOBDC, i.e. $Đ_{Xe}/r_c^2 = 2\times10^{-2}$ s^{-1}; $Đ_{Kr}/r_c^2 = 5\times10^{-2}$ s^{-1}. As anticipated the influence of intra-crystalline diffusion is seen to be of a minor nature. This conclusion is in line with those drawn by Wu et al.[15] on the basis of detailed experimental data on breakthroughs for CO_2/N_2, CO_2/CH_4, and CO_2/H_2 mixtures in Cu-TDPAT.

Comparing Xe/Kr Separations with Different MOFs

Let us compare the performance of different MOFs for separation of 20/80 Xe/Kr mixtures. Fig. S10 shows the breakthrough characteristics of 20/80 Xe/Kr mixtures in fixed beds packed with (a) Ni-DOBDC, (b) Ag@Ni-DOBDC (c) HKUST-1 (d) IRMOF-1 (e) $Co_3(HCOO)_6$ and (f) FMOFCu at 298 K. The simulations for Ni-DOBDC, Ag@Ni-DOBDC, HKUST-1 and IRMOF-1 assume thermodynamic equilibrium because the influence of diffusional limitations is expected to be of negligible importance as established in the foregoing section. For $Co_3(HCOO)_6$ and FMOFCu, the breakthrough simulations include intra-crystalline diffusion effects with the same diffusivity values as have been used to match the experimental data analyzed earlier. On the basis of the outlet gas compositions, we can determine the ppm Xe in the outlet gas as a function of the dimensionless time, τ, see Fig. S11. Let us arbitrarily

assume that the desired product Kr should have a purity corresponding to 1000 ppm Xe. Corresponding to this purity requirement we can determine the dimensionless breakthrough time, τ_{break}, at which the operation of the fixed bed needs to be stopped and regeneration started to recover pure Xe. From a material balance we can determine the productivity of Kr during the time interval 0 - τ_{break}. The productivities, expressed as mol of pure Kr produced per L of MOF are plotted in Fig. S12 as a function of the dimensionless breakthrough time, τ_{break}. The MOF with the highest productivity is Ag@Ni-DOBDC. Despite have the highest adsorption selectivity; $Co_3(HCOO)_6$ has a productivity that is significantly lower than that of Ag@Ni-DOBDC; it is also lower than that of Ni-DOBDC. The reasons for the lower productivity of $Co_3(HCOO)_6$ are two-fold: (a) lower uptake capacity, and (b) strong diffusional limitations. The low adsorption selectivities of IRMOF-1 and FMOFCu do not allow the production of Kr with the required purity levels.

Removal of Xe and Kr from Off-Gas Stream in Nuclear Plant

The removal and recovery of xenon (Xe) and krypton (Kr) from process off-gases from nuclear plants, typically present in concentrations of 400 ppm and 40 ppm, respectively, is an important problem.[1] Liu et al.[1] have presented isotherm and breakthrough data to demonstrate the efficacy of Ni-DOBDC for use in this separation task. For a process gas containing predominantly N_2, and containing impurities such as Xe (400 ppm), Kr (40 ppm), and CO_2 (400 ppm), the breakthrough simulations in Fig. S13 confirm that it is possible to recover Xe and Kr in nearly pure forms.

Conclusion

The following conclusions can be drawn on the basis of our analysis.

(1) The Xe/Kr separation characteristics of various MOFs depend on a combination of three separate factors: (a) adsorption selectivity, (b) uptake capacity, and (c) intra-crystalline diffusivity.

(2) For MOFs such as $Co_3(HCOO)_6$ and FMOFCu, in which the guest molecules are strongly confined, intra-crystalline diffusion effects are significant. Such diffusional effects result in distended breakthrough characteristics that have been observed in experimental measurements. Distended breakthroughs result in lower productivities.

(3) On the basis of our analysis, we conclude that Ag@Ni-DOBDC is the best MOF for Xe/Kr separations. $Co_3(HCOO)_6$ that has the highest Xe/Kr selectivity, has a significantly lower productivity than Ag@Ni-DOBDC because of strong diffusional influences.

Notation

b_A	dual-Langmuir-Freundlich constant for species *i* at adsorption site A, $Pa^{-\nu_i}$
b_B	dual-Langmuir-Freundlich constant for species *i* at adsorption site B, $Pa^{-\nu_i}$
c_i	molar concentration of species *i* in gas mixture, mol m^{-3}
c_{i0}	molar concentration of species *i* in gas mixture at inlet to adsorber, mol m^{-3}
$Đ_i$	Maxwell-Stefan diffusivity, m^2 s^{-1}
L	length of packed bed adsorber, m
n	number of species in the mixture, dimensionless
N_i	molar flux of species *i*, mol m^{-2} s^{-1}
p_i	partial pressure of species *i* in mixture, Pa
p_t	total system pressure, Pa
q_i	component molar loading of species *i*, mol kg^{-1}
$\bar{q}_i(t)$	*spatially averaged* component molar loading of species *i*, mol kg^{-1}
r_c	radius of crystallite, m
R	gas constant, 8.314 J mol^{-1} K^{-1}
t	time, s
T	absolute temperature, K
u	superficial gas velocity in packed bed, m s^{-1}
v	interstitial gas velocity in packed bed, m s^{-1}

Greek Letters

α	polarizability, cm^3
ε	voidage of packed bed, dimensionless
ρ	framework density, kg m^{-3}
τ	time, dimensionless

Subscripts

i	referring to component *i*
break	referring to breakthrough
t	referring to total mixture

References

(1) Liu, J.; Thallapally, P. K.; Strachan, D. Metal−Organic Frameworks for Removal of Xe and Kr from Nuclear Fuel Reprocessing Plants, *Langmuir* **2012**, *28*, 11584-11589.

(2) Liu, J.; Strachan, D. M.; Thallapally, P. K. Enhanced noble gas adsorption in Ag@MOF-74Ni, *Chem. Commun.* **2014**, *50*, 466-468.

(3) Gurdal, Y.; Keskin, S. Atomically Detailed Modeling of Metal Organic Frameworks for Adsorption, Diffusion, and Separation of Noble Gas Mixtures, *Ind. Eng. Chem. Res.* **2012**, *51*, 7373-8382.

(4) Fernandez, C. A.; Liu, J.; Thallapally, P. K.; Strachan, D. M. Switching Kr/Xe Selectivity with Temperature in a Metal−Organic Framework, *J. Am. Chem. Soc.* **2012**, *134*, 9046-9049.

(5) Wang, H.; Yao, K.; Zhang, Z.; Jagiello, J.; Gong, Q.; Han, Y.; Li, J. The First Example of Commensurate Adsorption of Atomic Gas in a MOF and Effective Separation of Xenon from Other Noble Gases, *Chem. Sci.* **2014**, *5*, 620-624.

(6) Krishna, R.; van Baten, J. M. A molecular dynamics investigation of the diffusion characteristics of cavity-type zeolites with 8-ring windows, *Microporous Mesoporous Mater.* **2011**, *137*, 83-91.

(7) van den Bergh, J.; Zhu, W.; Gascon, J.; Moulijn, J. A.; Kapteijn, F. Separation and Permeation Characteristics of a DD3R Zeolite Membrane, *J. Membr. Sci.* **2008**, *316*, 35-45.

(8) Myers, A. L.; Prausnitz, J. M. Thermodynamics of mixed gas adsorption, *A.I.Ch.E.J.* **1965**, *11*, 121-130.

(9) Krishna, R.; Long, J. R. Screening metal-organic frameworks by analysis of transient breakthrough of gas mixtures in a fixed bed adsorber, *J. Phys. Chem. C* **2011**, *115*, 12941-12950.

(10) Krishna, R. The Maxwell-Stefan Description of Mixture Diffusion in Nanoporous Crystalline Materials, *Microporous Mesoporous Mater.* **2014**, *185*, 30-50.

(11) Krishna, R.; Baur, R. Modelling issues in zeolite based separation processes, *Sep. Purif. Technol.* **2003**, *33*, 213-254.

(12) Krishna, R.; van Baten, J. M. Investigating the potential of MgMOF-74 membranes for CO_2 capture, *J. Membr. Sci.* **2011**, *377*, 249-260.

(13) He, Y.; Krishna, R.; Chen, B. Metal-Organic Frameworks with Potential for Energy-Efficient Adsorptive Separation of Light Hydrocarbons, *Energy Environ. Sci.* **2012**, *5*, 9107-9120.

(14) Liu, J.; Tian, J.; Thallapally, P. K.; McGrail, B. P. Selective CO_2 Capture from Flue Gas Using Metal−Organic Frameworks - A Fixed Bed Study, *J. Phys. Chem. C* **2012**, *116*, 9575-9581.

(15) Wu, H.; Yao, K.; Zhu, Y.; Li, B.; Shi, Z.; Krishna, R.; Li, J. Cu-TDPAT, an *rht*-type Dual-Functional Metal–Organic Framework Offering Significant Potential for Use in H_2 and Natural Gas Purification Processes Operating at High Pressures, *J. Phys. Chem. C* **2012**, *116*, 16609-16618.

(16) Chmelik, C.; Kärger, J.; Wiebcke, M.; Caro, J.; van Baten, J. M.; Krishna, R. Adsorption and Diffusion of Alkanes in CuBTC Crystals Investigated Using Infrared Microscopy and Molecular Simulations, *Microporous Mesoporous Mater.* **2009**, *117*, 22-32.

(17) Krishna, R.; van Baten, J. M. Onsager coefficients for binary mixture diffusion in nanopores, *Chem. Eng. Sci.* **2008**, *63*, 3120-3140.

(18) Krishna, R.; van Baten, J. M. Unified Maxwell-Stefan description of binary mixture diffusion in micro- and meso- porous materials, *Chem. Eng. Sci.* **2009**, *64*, 3159-3178.

(19) Krishna, R.; van Baten, J. M. Investigating the Relative Influences of Molecular Dimensions and Binding Energies on Diffusivities of Guest Species Inside Nanoporous Crystalline Materials *J. Phys. Chem. C* **2012**, *116*, 23556-23568.

(20) Dietzel, P. D. C.; Besikiotis, V.; Blom, R. Application of metal–organic frameworks with coordinatively unsaturated metal sites in storage and separation of methane and carbon dioxide, *J. Mater. Chem.* **2009**, *19*, 7362-7370.

Supporting Figures

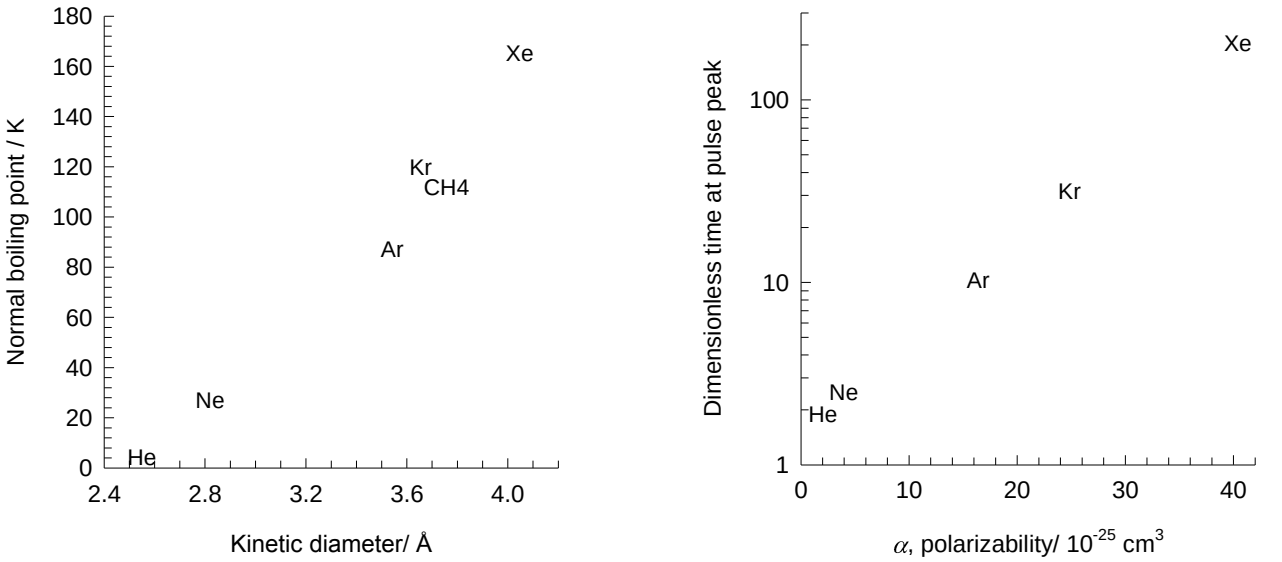

Fig. S1. Comparison of molar masses, kinetic diameters, boiling points and polarizabilities of noble gases (He, Ne, Ar, Kr, Xe). Also presented, for reference purposes, are the properties of CH_4.

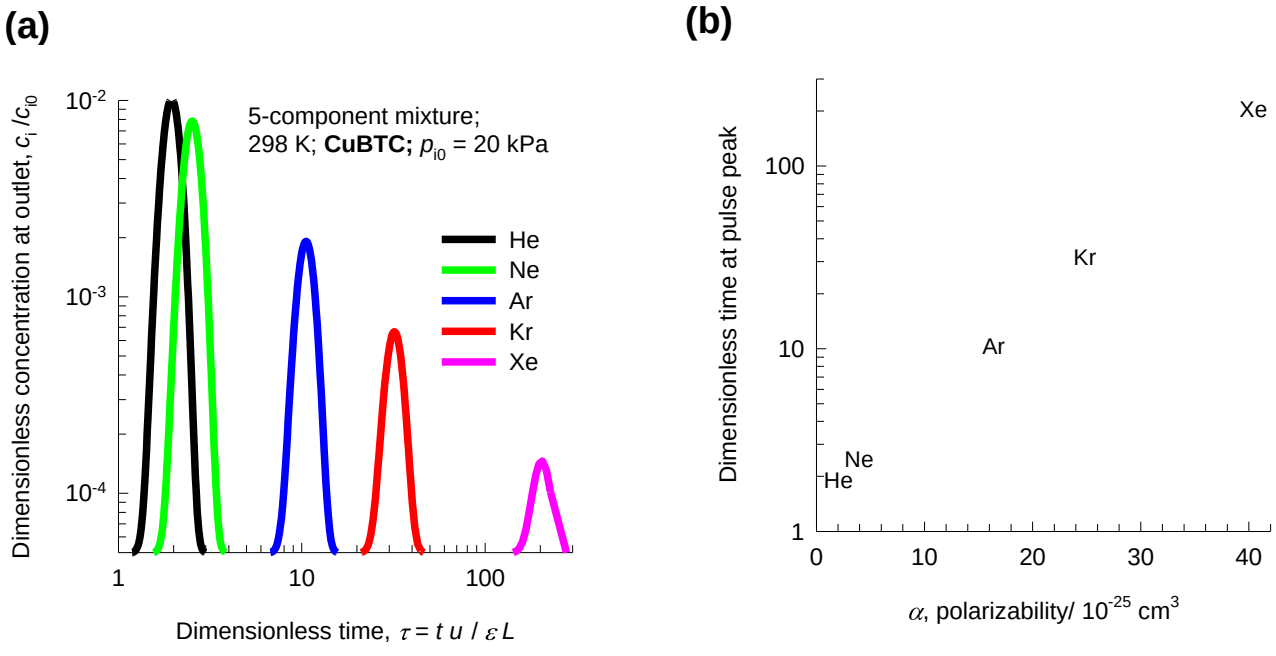

Fig. S2. (a) Pulse chromatographic simulations for separation of a 5-component mixture of noble gases He/Ne/Ar/Kr/Xe in a fixed bed of HKUST-1 operating at 298 K and a total pressure of 100 kPa. The breakthrough simulations reported here use the parameter values: L = 2 m; voidage of bed, ε = 0.4; interstitial gas velocity, v = 0.05 m/s; superficial gas velocity, u = 0.02 m/s. In pulse chromatographic simulations we take the pulse duration t_0 = 0.2 s. The pure component isotherms are obtained from

Configurational-Bias Monte Carlo (CBMC) simulation data from published works.[3, 16-18] (b) Plot of the dimensionless "peak" times for each pulse as a function of the polarizability.

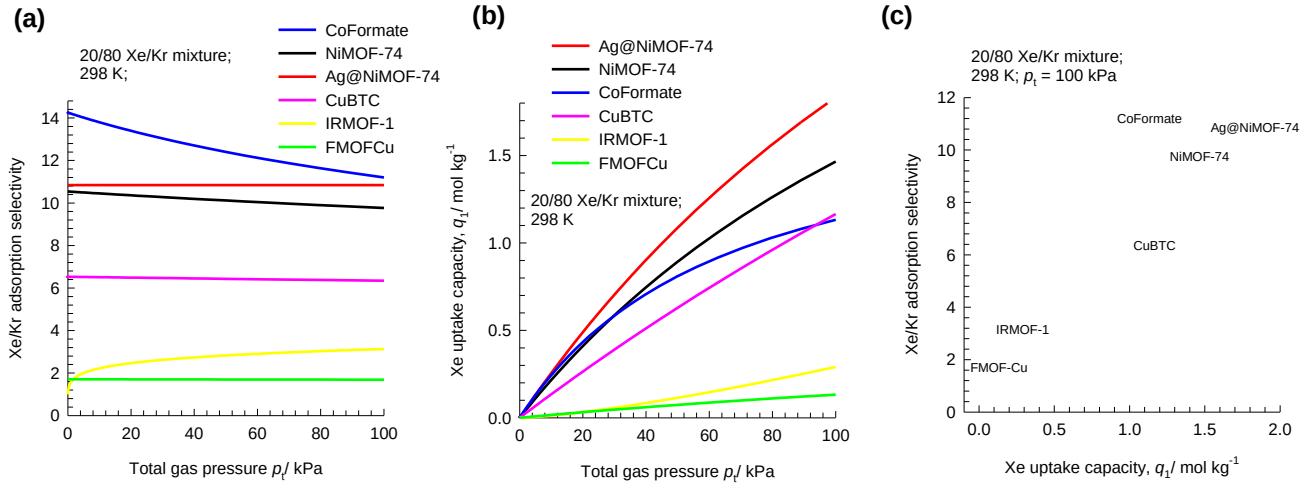

Fig. S3. Comparison of (a) adsorption selectivity (S_{ads}) and (b) Xe uptake capacities, q_1, for Ni-DOBDC (NiMOF-74), Ag@Ni-DOBDC (Ag@NiMOF-74), HKUST-1 (Cu-BTC), IRMOF-1, FMOFCu, and $Co_3(HCOO)_6$ (Co Formate) for 20/80 Xe(1)/Kr(2) mixtures as a function of the total gas pressure. (c) Plot of S_{ads} vs q_1 at 100 kPa total pressure. The calculations presented here are based on the Ideal Adsorbed Solution Theory (IAST) of Myers and Prausnitz.[8] The pure component isotherm data used in the IAST calculations are from literature sources: Ni-DOBDC (NiMOF-74),[1, 2] Ag@Ni-DOBDC (Ag@NiMOF-74),[2] HKUST-1 (Cu-BTC),,[3] IRMOF-1,[3] FMOFCu,[4] and $Co_3(HCOO)_6$ (Co Formate).[5]

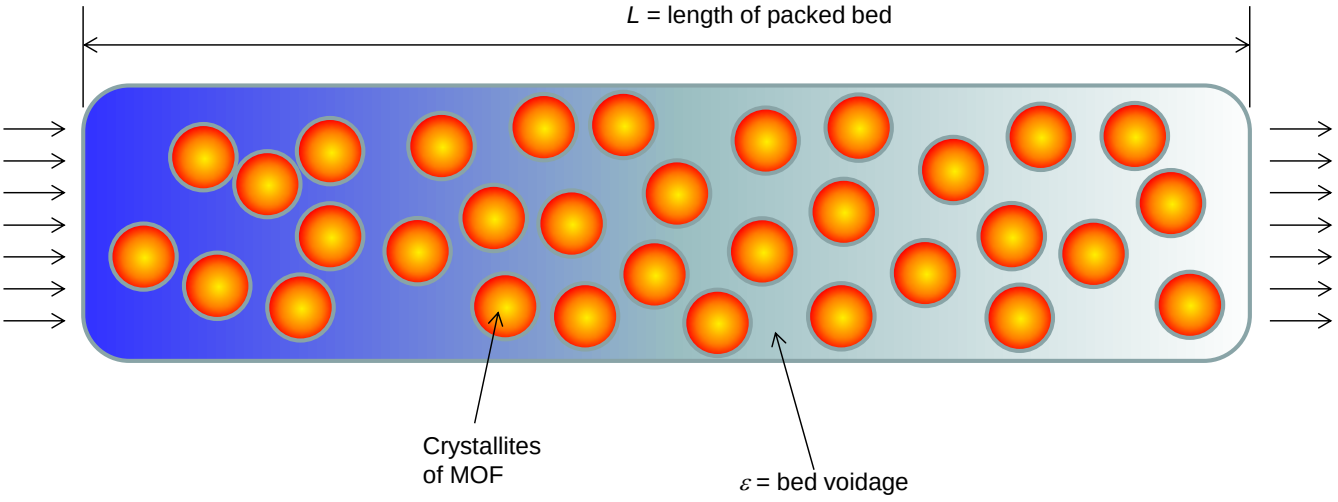

Fig. S4. Schematic of a packed bed adsorber.

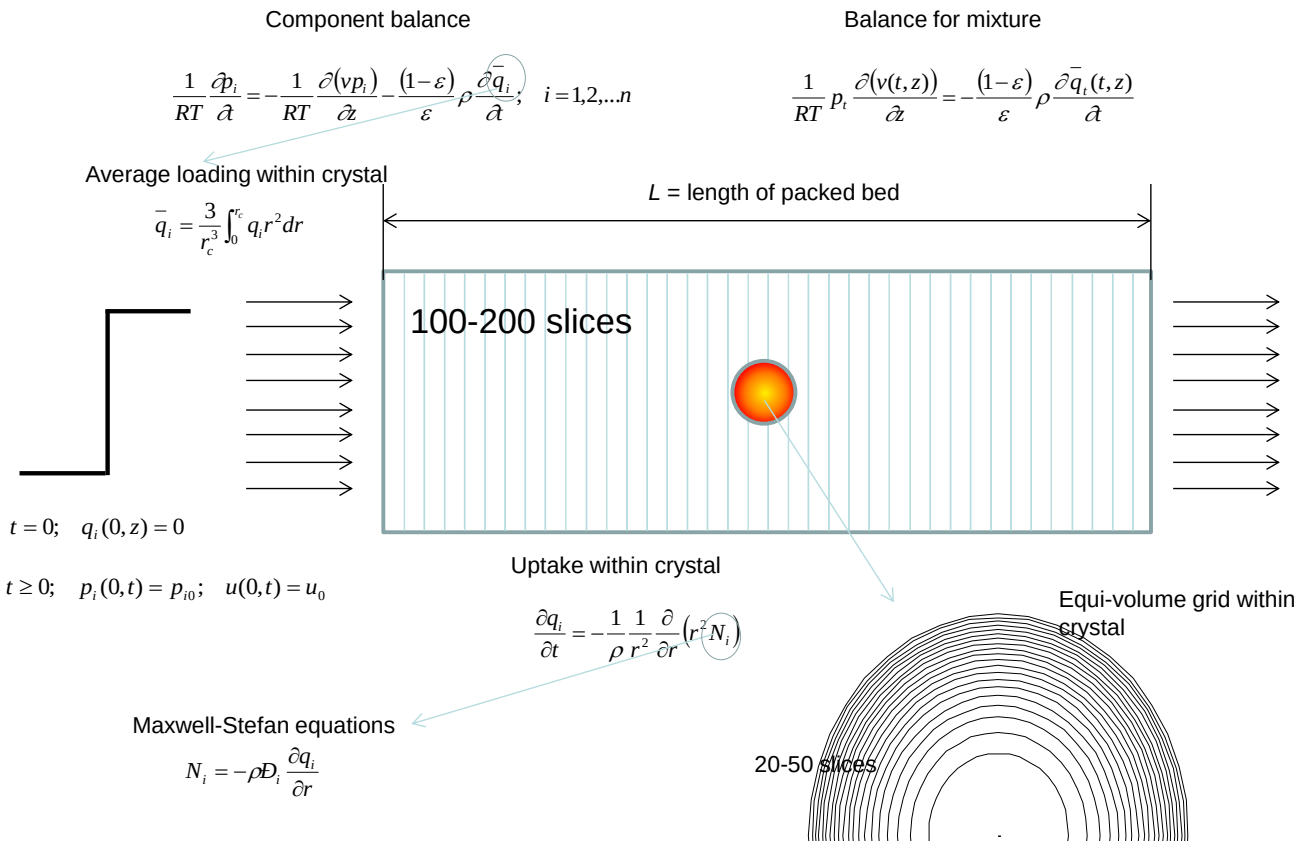

Fig. S5. Summary of model equations describing packed bed adsorber, along with discretization scheme.

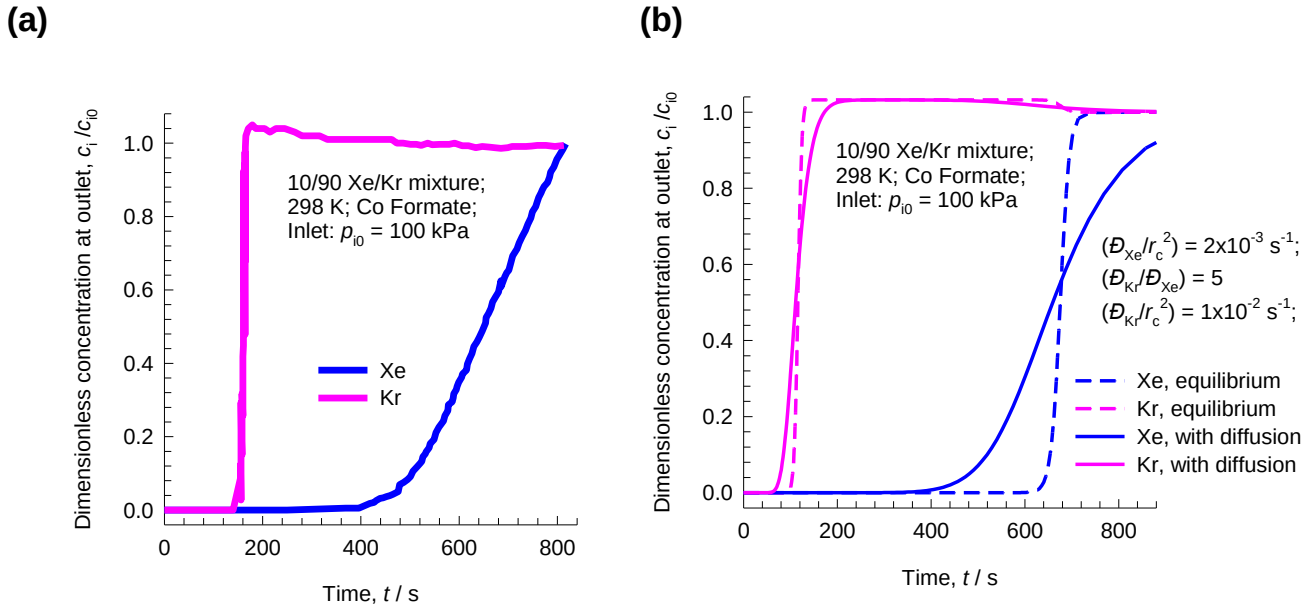

Fig. S6. (a) Experimental breakthroughs for 10/90 Xe/Kr mixtures at 298 K and 100 kPa in a bed packed with $Co_3(HCOO)_6$; the data are scanned from Fig. S9 of the Supporting Information accompanying the paper by Wang et al.[5] (b) Simulations without intra-crystalline diffusion limitations (i.e. equilibrium between bulk gas and crystal at any location and invoking Equation (11) (indicated by dashed lines) are

compared with breakthrough simulations (continuous solid lines) that include intra-crystalline diffusion effects using equation (**5**). The chosen diffusivity values are $Đ_{Xe}/r_c^2 = 2\times10^{-3}$ s^{-1}; $Đ_{Kr}/r_c^2 = 1\times10^{-2}$ s^{-1}. The pure component isotherm data used in the IAST calculations are from Wang et al.[5]

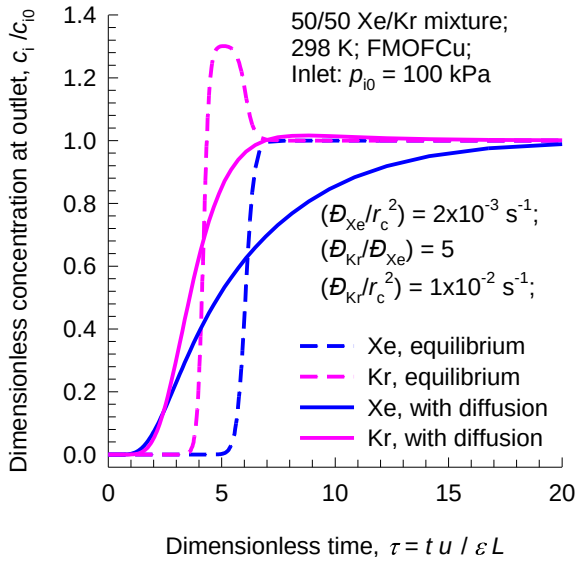

Fig. S7. Simulations without intra-crystalline diffusion limitations (i.e. equilibrium between bulk gas and crystal at any location and invoking Equation (11) (indicated by dashed lines) are compared with breakthrough simulations (continuous solid lines) that include intra-crystalline diffusion effects using equation (**5**). The chosen diffusivity values are $Đ_{Xe}/r_c^2 = 2\times10^{-3}$ s^{-1}; $Đ_{Kr}/r_c^2 = 1\times10^{-2}$ s^{-1}. The pure component isotherm data used in the IAST calculations are from Fernandez et al.[4] For the breakthrough simulations reported here we use the parameter values: L = 0.3 m; voidage of bed, ε = 0.4; interstitial gas velocity, v = 0.1 m/s; superficial gas velocity, u = 0.04 m/s.

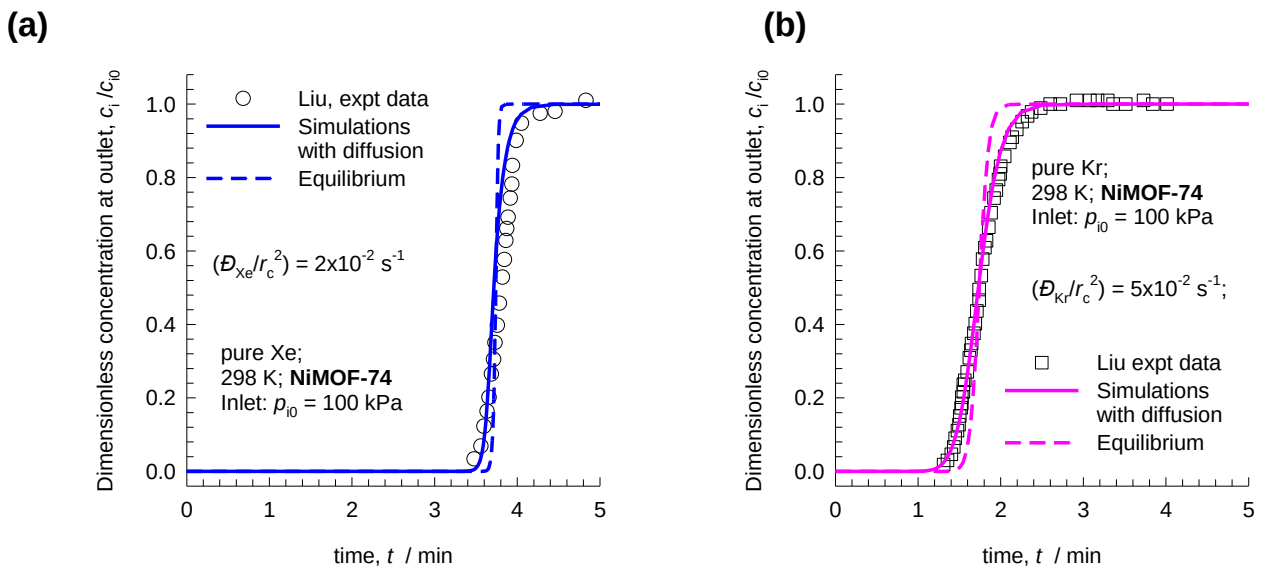

Fig. S8. (a, b) Comparison of experimental breakthroughs with simulations including intra-crystalline diffusion effects (continuous solid lines) with chosen diffusivity values are $Đ_{Xe}/r_c^2 = 2\times10^{-2}$ s^{-1}; $Đ_{Kr}/r_c^2 = 5\times10^{-2}$ s^{-1}. The dashed lines in (a, b) are simulations in which intra-crystalline diffusional effects are ignored.

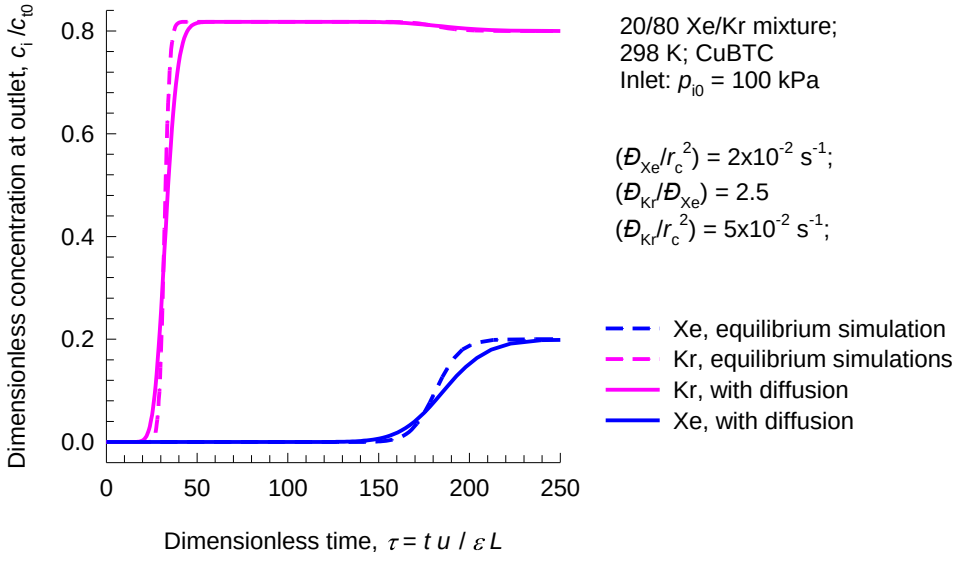

Fig. S9. Simulations without intra-crystalline diffusion limitations (i.e. equilibrium between bulk gas and crystal at any location and invoking Equation (11) (indicated by dashed lines) are compared with breakthrough simulations (continuous solid lines) that include intra-crystalline diffusion effects using

equation (**5**). The chosen diffusivity values are $Đ_{Xe}/r_c^2 = 2\times10^{-2}$ s^{-1}; $Đ_{Kr}/r_c^2 = 5\times10^{-2}$ s^{-1}. The pure component isotherm data used in the IAST calculations are from Gurdal and Keskin.[3] For the breakthrough simulations reported here we use the parameter values: L = 0.3 m; voidage of bed, ε = 0.4; interstitial gas velocity, v = 0.1 m/s; superficial gas velocity, u = 0.04 m/s.

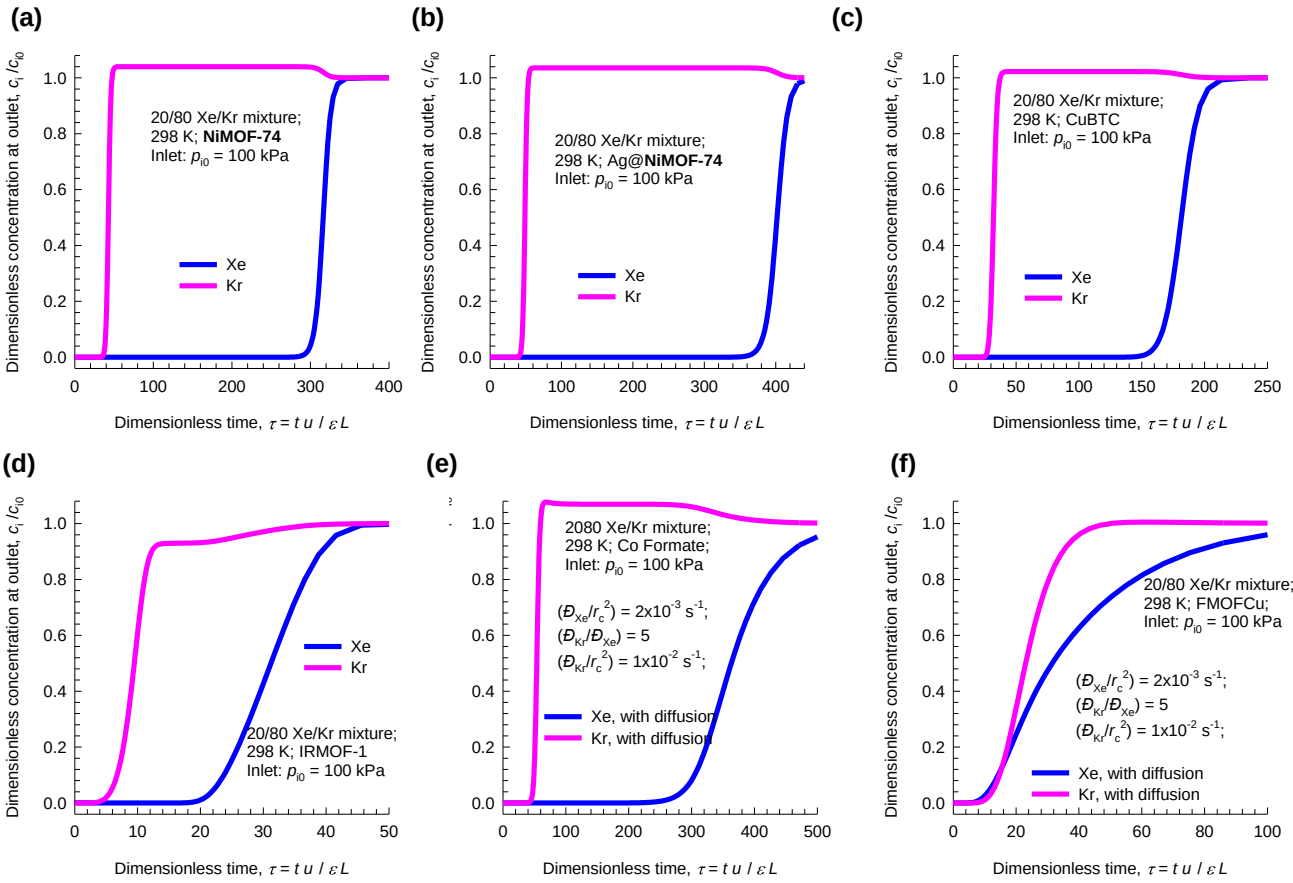

Fig. S10. Breakthrough characteristics of 20/80 Xe/Kr mixtures in fixed beds packed with (a) Ni-DOBDC (NiMOF-74), (b) Ag@Ni-DOBDC (Ag@NiMOF-74), (c) HKUST-1 (CuBTC), (d) IRMOF-1, (e) $Co_3(HCOO)_6$ (Co-formate) and (f) FMOFCu at 298 K. The total pressure at the inlet is 100 kPa in all cases. The breakthrough simulations in (a) Ni-DOBDC (NiMOF-74), (b) Ag@Ni-DOBDC (Ag@NiMOF-74), (c) HKUST-1 (CuBTC), (d) IRMOF-1 assume thermodynamic equilibrium, i.e. invoking Equation (11). For (e) $Co_3(HCOO)_6$ (Co-formate), and (f) FMOFCu the breakthrough simulations include intra-crystalline diffusion effects with the chosen diffusivity values $Đ_{Xe}/r_c^2 = 2\times10^{-3}$ s^{-1}; $Đ_{Kr}/r_c^2 = 1\times10^{-2}$ s^{-1}. For the breakthrough simulations reported here we use the parameter values: L = 0.3 m; voidage of bed, ε = 0.4; interstitial gas velocity, v = 0.1 m/s; superficial gas velocity, u = 0.04 m/s.

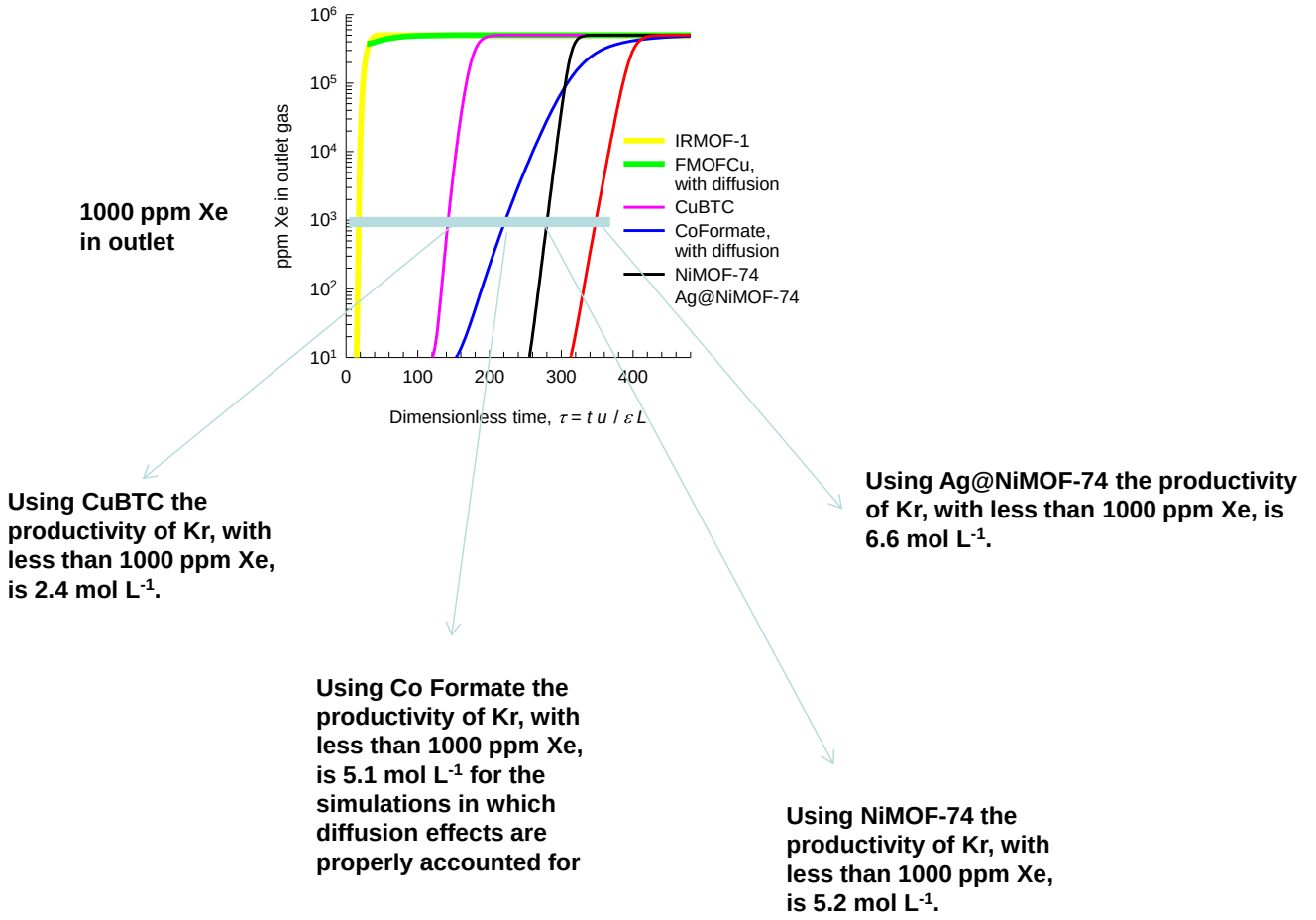

Fig. S11. Xe (in ppm level) in the outlet gas mixture of 20/80 Xe/Kr mixtures in fixed beds packed with (a) Ni-DOBDC (NiMOF-74), (b) Ag@Ni-DOBDC (Ag@NiDOBDC), (c) HKUST-1 (CuBTC), (d) IRMOF-1, (e) $Co_3(HCOO)_6$ (Co-formate) and (f) FMOFCu at 298 K. The calculations are based on the breakthrough simulations presented in Fig. S10.

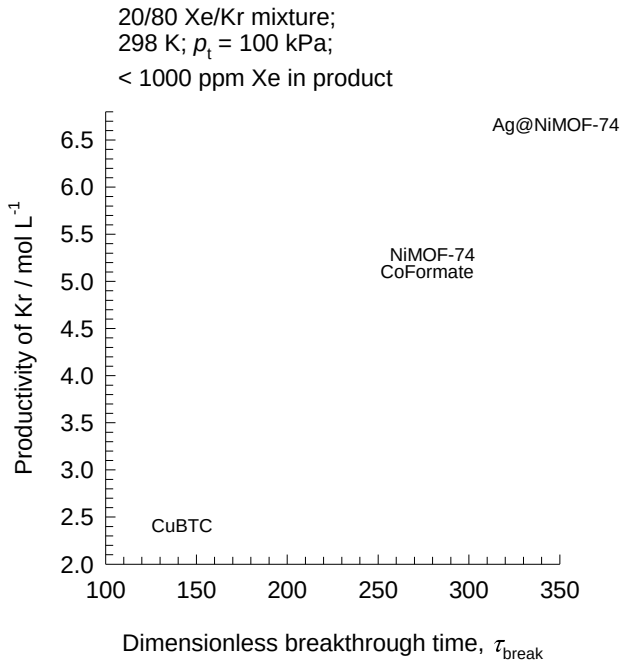

Fig. S12. Dependence of the productivity of pure Kr (with < 1000 ppm Xe), expressed in mol of product per L of MOF, as a function of the dimensionless breakthrough time, τ_{break}.

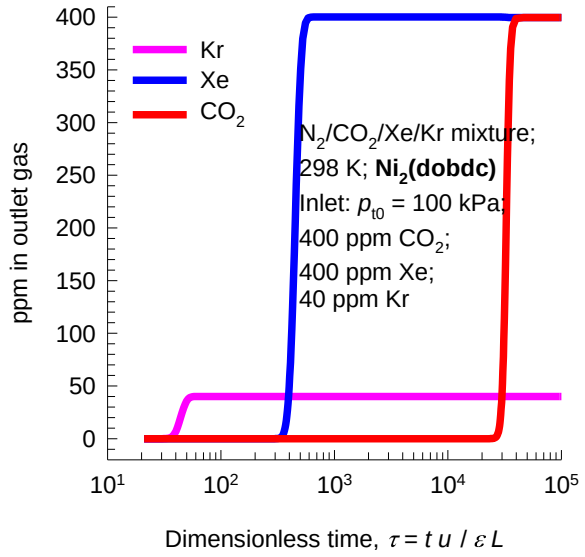

Fig. S13. Breakthrough characteristics of 400/400/40/10^6 CO_2/Xe/Kr/N_2 mixtures in Ni-DOBDC at 298 K. The total pressure at the inlet is 100 kPa. The breakthrough simulations, assume thermodynamic equilibrium, i.e. invoking Equation (11). The pure component isotherm data for CO_2, and N_2 in Ni_2(dobdc) are those reported by Krishna and van Baten[19], based on the data of Dietzel et al.[20] The pure component isotherm data for Xe and Kr are from Liu et al.[1] Other parameter values are: L = 0.3 m; voidage of bed, ε = 0.4; interstitial gas velocity, v = 0.1 m/s.